Comput Mech (2017) 59:37–72
DOI 10.1007/s00466-016-1334-7

ORIGINAL PAPER

A unified quadrature-based superconvergent finite element formulation for eigenvalue computation of wave equations

Dongdong Wang[1] · **Xiwei Li**[1] · **Feixu Pan**[1]

Received: 28 June 2016 / Accepted: 14 September 2016 / Published online: 3 November 2016

Abstract A simple and unified finite element formulation is presented for superconvergent eigenvalue computation of wave equations ranging from 1D to 3D. In this framework, a general method based upon the so called α mass matrix formulation is first proposed to effectively construct 1D higher order mass matrices for arbitrary order elements. The finite elements discussed herein refer to the Lagrangian type of Lobatto elements that take the Lobatto points as nodes. Subsequently a set of quadrature rules that exactly integrate the 1D higher order mass matrices are rationally derived, which are termed as the superconvergent quadrature rules. More importantly, in 2D and 3D cases, it is found that the employment of these quadrature rules via tensor product simultaneously for the mass and stiffness matrix integrations of Lobatto elements produces a unified superconvergent formulation for the eigenvalue or frequency computation without wave propagation direction dependence, which usually is a critical issue for the multidimensional higher order mass matrix formulation. Consequently the proposed approach is capable of computing arbitrary frequencies in a superconvergent fashion. Meanwhile, numerical implementation of the proposed method for multidimensional problems is trivial. The effectiveness of the proposed methodology is systematically demonstrated by a series of numerical examples. Numerical results revealed that a superconvergence with $2(p+1)$th order of frequency accuracy is achieved by the present unified formulation for the pth order Lobatto element.

✉ Dongdong Wang
ddwang@xmu.edu.cn

[1] Department of Civil Engineering, Xiamen University, Xiamen 361005, Fujian, China

Keywords Eigenvalue · Wave equation · Superconvergence · α Mass matrix · Higher order mass matrix · Superconvergent quadrature rule · Lobatto element

1 Introduction

The eigenvalue problems arising from wave equations represent a large class of important engineering problems, such as free vibrations of rod, string, membrane and acoustic problems, etc. Within the context of the finite element method, based upon the weak formulation, the eigenvalue problems are converted into their discrete counterparts characterized by the mass and stiffness matrices [1,2]. Quite often the stiffness matrix is formulated by standard Gauss quadrature, while there are several candidates for the mass matrix. The widely used consistent mass matrix [3] is directly derived from the weak form. On the other hand, the ad hoc lumped mass matrix with diagonal terms only is preferred due to its efficiency and suitability for explicit transient analysis. The row sum method [1], nodal quadrature method [1,4] and the HRZ diagonal scaling method [5] are commonly used to generate a lumped mass matrix. These mentioned mass lumping techniques yield identical lumped mass matrices for the tensor product based Lagrangian elements. For the one dimensional (1D) cubic element, the nodal quadrature method is not applicable for the Lagrangian element with equally spaced nodes, and Fried and Malkus [4] pointed out that when the interior nodes are placed at $\pm\sqrt{5}/5$, the nodal quadrature rule yields a lumped mass matrix with 6th order of frequency accuracy that is the same as its consistent counterpart. This type of element essentially belongs to the family of Lobatto elements [6,7] whose shape functions interpolate the Lobatto points [8], which are frequently used in the spectral methods [9–11]. In [12], the error in the eigenvalue or

frequency of wave equations has been discussed in detail. Excellent summaries and reviews on the mass matrices can be found in [13–15], among others.

Nonetheless, it has been shown that both consistent and lumped mass matrices may not be optimal for eigenvalue computation, e.g., an average for the consistent and lumped mass matrices for 1D linear element gives a superconvergent result, which is called a higher order mass matrix with excellent dispersion property [16–22]. Thus the construction of higher order mass matrices is of great interest for finite element eigenvalue computation. Meanwhile, in order to improve the accuracy of eigenvalue or frequency analysis, various methods have also been developed. For example, Gurtin [23] and Stavrinidis et al. [13] proposed the velocity shape functions to construct the mass matrix. Hansson and Sandberg [24] presented a method for mass matrix construction through minimizing the modal error. An inverse method was given by Ahmadian et al. [25] and Ahmadian and Farughi [26] to minimize the discretization error in mass and stiffness matrices. The method of selective mass scaling has been investigated by Olovsson et al. [27], Tkachuk and Bischoff [28], and Cocchetti et al. [29], etc. Felippa [30–32] proposed a template method to customize the construction of mass-stiffness pairs. This approach is very general with broad applicability, while it may involve the optimization of many parameters, which could be very challenging even for two dimensional (2D) problems, let alone three dimensional (3D) problems. This point is also illustrated by the recent review article by Felippa et al. [15]. Moreover, Fried and Chavez [21] further showed the consistent, lumped and higher order mass matrices can be put into a linear function of two mass matrices with an adjustable parameter. This parameter can be tuned to achieve a higher order mass matrix with frequency superconvergence, which is demonstrated for 1D linear, quadratic, 2D linear triangle and four-node bilinear square membrane elements, respectively. Later Fried and Leong [33] also presented a method of Rayleigh quotient correction for the higher order mass matrix formulation. Despite of these significant advances on the higher order mass matrix formulation, most existing results are obtained on a case-by-case basis and it seems that there is still a lack of simple and unified ways to develop superconvergent formulations for arbitrary order elements, especially for multidimensional problems. Furthermore, numerical experiments also show that the multidimensional higher order mass matrix formulation exhibits a strong dependence on wave propagation directions, and provides superconvergence only for certain frequencies.

On the other hand, in the context of isogeometric analysis that provides a seamless integration of computer aided geometry design and the finite element analysis [34–36], 1D, 2D and 3D isogeometric higher order mass matrices have been developed to achieve superconvergent frequency computation [37–39]. The isogeometric analysis employs the smoothing and convex B-spline or non-uniformed rational B-spline basis functions, thus the consistent mass matrix has non-negative entries with sound frequency spectra, but the desired accuracy is lost when a lumped mass matrix is used [35,36]. In order to construct an isogeometric higher order mass matrix, a new reduced bandwidth matrix that has an equal order of accuracy as its consistent counterpart was introduced in [37]. Subsequently an optimal combination of the reduced bandwidth and consistent mass matrices results in a higher order mass matrix. In addition, to remove the wave propagation direction dependence issue, the mass combination parameter is optimized as a function of the wave propagation angles [38,39]. This approach ensures a superconvergent computation of arbitrary frequencies. However, the mass combination parameter has to be adjusted for the frequencies corresponding to different wave propagation directions, which is not preferable from the numerical implementation point of view.

This work aims to develop a simple and unified finite element formulation that enables a superconvergent frequency computation of wave equations for arbitrary order elements without the issue of wave propagation direction dependence. The present formulation is based upon the Lagrangian type of Lobatto elements, which are simply called Lobatto elements for convenience in the subsequent development. As the first step, an α mass matrix is proposed to formulate 1D higher order mass matrices for arbitrary order elements. Theoretical proofs are presented for linear and quadratic elements that their higher order mass matrices with superconvergence can be obtained by letting α be the optimal value of $\alpha_{opt} = p + 1$, where p is the order of the given element. This result is then used to develop the higher order mass matrices for cubic and quartic elements, whose superconvergence are validated by numerical examples. Thereafter, for 2D bilinear elements, it is shown that the desired superconvergence without wave propagation direction dependence can be achieved if the same quadrature rule is employed for both mass and stiffness matrices. More importantly, this quadrature rule turns out to be the exact integration rule for 1D higher order mass matrix of linear element. This observation is further proved for 3D trilinear element. Subsequently a generalization of this methodology to higher order elements is presented, in particular, the superconvergent quadrature rules for quadratic, cubic and quartic elements are given in detail. Consequently, a unified quadrature-based superconvergent formulation is established for multidimensional problems. Due to its quadrature nature, numerical implementation of this formulation is trivial. The efficacy of the proposed superconvergent formulation is systematically verified through numerical examples.

An outline of the remainder of this paper is as follows. Section 2 briefly summarizes the model problem considered

herein and its finite element discretization. The motivation and objective of this work is described in Sect. 3. Subsequently, in Sect. 4, a unified formulation is developed to construct 1D higher order mass matrices based upon Lobatto elements. The multidimensional unified quadrature-based superconvergent formulation is presented in Sect. 5. The superconvergent performance of the proposed method is assessed in Sect. 6 by a set of 2D and 3D numerical examples. Finally conclusions are drawn in Sect. 7.

2 Model problem and basic finite element equations

2.1 Model problem

In this work, we consider the following classical wave equation:

$$\ddot{u}(\boldsymbol{x},t) = c^2\nabla^2 u(\boldsymbol{x},t),\ \nabla^2 = \sum_{i=1}^{n_{sd}} \frac{\partial^2}{\partial x_i^2} \tag{1}$$

where $u(\boldsymbol{x},t)$ is the field variable that can be the longitudinal displacement for 1D rod vibration, the transverse displacement for 2D membrane vibration, or the acoustic pressure for 3D acoustic problem. $\boldsymbol{x} = \{x, y, z\}^T$, t denotes the time and c is the wave speed. The superposed dot and the subscript comma represent temporal and spatial differentiations, respectively. ∇^2 stands for the Laplace operator and n_{sd} is the spatial dimension.

According to the standard harmonic assumption, the field variable $u(\boldsymbol{x},t)$ can be expressed as:

$$u(\boldsymbol{x},t) = \hat{u}\exp\left[\iota(\boldsymbol{k}\cdot\boldsymbol{x} - \omega t)\right],\ \iota = \sqrt{-1} \tag{2}$$

where $\hat{u}$ denotes the wave amplitude, $\boldsymbol{k} = \{k_x, k_y, k_z\}^T$, k_x, k_y and k_z represent the wave numbers in x, y and z directions, respectively. ω is the continuum angular frequency. Substituting Eqs. (2) into (1) yields:

$$\omega = \|\boldsymbol{k}\|\, c,\quad \|\boldsymbol{k}\| = \sqrt{k_x^2 + k_y^2 + k_z^2} \tag{3}$$

The finite element analysis is based upon the weak form of Eq. (1):

$$\int_\Omega \delta u \ddot{u} d\Omega + \int_\Omega c^2(\nabla\delta u)\cdot(\nabla u) d\Omega = 0 \tag{4}$$

in which Ω denotes the problem spatial domain, ∇ is the gradient operator.

2.2 Basic finite element equations

In finite element analysis, the problem domain Ω is partitioned into an assembly of individual elements Ω^e, i.e., $\Omega = \bigcup_{e=1}^{n_{el}} \Omega^e$, n_{el} denotes the total number of elements. In each element, the approximation of the field variable $u(\boldsymbol{x},t)$, denoted by $u^h(\boldsymbol{x},t)$, takes the following form:

$$u^h(\boldsymbol{x},t) = \sum_{a=1}^{n_{en}} N_a(\boldsymbol{\xi}) d_a(t) \tag{5}$$

where $N_a(\boldsymbol{\xi})$ is the shape function associated with the node $\boldsymbol{x}_a$, which is often defined on the natural coordinate $\boldsymbol{\xi}$. n_{en} denotes the number of nodes per element and $d_a(t)$ is the nodal degree of freedom. The lowercase subscripts represent the local node numberings in the element level, while the uppercase subscripts used later on denote the global node numberings.

Introducing Eqs. (5) into (4) within the Bubnov-Galerkin finite element formulation gives the following standard discrete equation:

$$\boldsymbol{M}\ddot{\boldsymbol{d}} + \boldsymbol{K}\boldsymbol{d} = \boldsymbol{0} \tag{6}$$

where $\boldsymbol{M}$ and $\boldsymbol{K}$ are the global mass and stiffness matrices, $\boldsymbol{d}$ is the vector consisting of the global nodal degrees of freedom, which can be assembled by their element counterparts:

$$\boldsymbol{M} = \underset{e=1}{\overset{n_{el}}{A}}[\boldsymbol{M}^e],\ \boldsymbol{K} = \underset{e=1}{\overset{n_{el}}{A}}[\boldsymbol{K}^e],\ \boldsymbol{d} = \underset{e=1}{\overset{n_{el}}{A}}[\boldsymbol{d}^e] \tag{7}$$

in which A is the local-global assembly operator [1]. The element mass matrix $\boldsymbol{M}^e$ and stiffness matrix $\boldsymbol{K}^e$ have the following expressions:

$$M_{ab}^e = \int_{\Omega^e} N_a N_b d\Omega \tag{8}$$

$$K_{ab}^e = c^2 \int_{\Omega^e} (\nabla N_a)\cdot(\nabla N_b) d\Omega \tag{9}$$

Explicit forms of $\boldsymbol{M}^e$ and $\boldsymbol{K}^e$ will be discussed later when we investigate specific elements. Further invoking the harmonic form of $\boldsymbol{d}(t) = \boldsymbol{\phi}\exp(\iota\omega^h t)$ in Eq. (6) yields the following typical eigenvalue problem:

$$\boldsymbol{K}\boldsymbol{\phi} = (\omega^h)^2\boldsymbol{M}\boldsymbol{\phi} \tag{10}$$

where ω^h is the semi-discrete frequency and $\boldsymbol{\phi}$ is the corresponding mode.

Quite often the relative error between the semi-discrete frequency ω^h and the continuum frequency ω is used as

an accuracy measure of finite element method. This error, denoted by e_f can be written as:

$$e_f = \frac{\omega^h}{\omega} - 1 \tag{11}$$

According to [1,12], the error in frequency for the conventional finite element formulation is:

$$e_f \approx O(h^{2p}) \tag{12}$$

where p is the completeness order of the finite element shape functions. Here we would like to develop a unified finite element approach that is capable of computing the frequencies with an error of $O(h^{2(p+1)})$ for both 1D and multidimensional problems, i.e., the frequency convergence rate increases from $2p$ of the conventional finite element formulation to $2(p+1)$ for the proposed formulation. In other words, a superconvergence is achieved for the frequency computation.

3 Motivation and objective

In this section we illustrate the motivation of our subsequent development. In the finite element setting, it has been shown that higher order mass matrix can be used to compute the frequencies with superconvergence, in comparison with the consistent and lumped mass formulations. Take 1D rod vibration as an example, for a typical two node linear element $[x_1^e,\ x_2^e]$ with length h, the higher order mass (HOM) matrix $\boldsymbol{M}^{eh}$ can be established as an average of the consistent mass (CM) matrix $\boldsymbol{M}^{ec}$ and the lumped mass (LM) matrix $\boldsymbol{M}^{el}$ [1,16,21]:

$$\begin{aligned}\boldsymbol{M}^{eh} &= \frac{1}{2}\boldsymbol{M}^{ec} + \frac{1}{2}\boldsymbol{M}^{el} \\ &= \frac{1}{2}\times\frac{h}{6}\begin{bmatrix}2&1\\1&2\end{bmatrix} + \frac{1}{2}\times\frac{h}{2}\begin{bmatrix}1&0\\0&1\end{bmatrix} \\ &= \frac{h}{12}\begin{bmatrix}5&1\\1&5\end{bmatrix}\end{aligned} \tag{13}$$

where without loss of generality, the material density and cross section area are all assumed to be unity. When the standard stiffness matrix is employed, it turns out that the frequency accuracy for HOM is $O(h^4)$, while only $O(h^2)$ is observed for both CM and LM [12]. Similarly, a quadratic higher order mass matrix with 6th order of accuracy can also be expressed as an optimal linear combination of the corresponding consistent and lumped mass matrices [21]:

$$\begin{aligned}\boldsymbol{M}^{eh} &= \frac{1}{3}\boldsymbol{M}^{ec} + \frac{2}{3}\boldsymbol{M}^{el} \\ &= \frac{1}{3}\times\frac{h}{30}\begin{bmatrix}4&2&-1\\2&16&2\\-1&2&4\end{bmatrix} + \frac{2}{3}\times\frac{h}{6}\begin{bmatrix}1&0&0\\0&4&0\\0&0&1\end{bmatrix} \\ &= \frac{h}{90}\begin{bmatrix}14&2&-1\\2&56&2\\-1&2&14\end{bmatrix}\end{aligned} \tag{14}$$

By contrast, the quadratic CM and LM are 4th order accurate. This again demonstrates a superconvergence for HOM.

Obviously, HOM is of great importance for the frequency computation. However, it is yet unclear that the combination of consistent and lumped mass matrices would always be able to produce a higher order mass matrix. Actually, in [37–39] it is pointed that two matrices with equal order of accuracy are necessary to yield a higher order mass matrix through optimal linear combination. At the same time, a straightforward computational experiment shows that the standard 1D cubic and quartic Lagrangian elements with equal nodal spacing do not give the same order of accuracy for CM and LM. This is illustrated in Fig. 1, where the convergence of the fundamental frequency for the fixed-fixed rod problem using the standard cubic and quartic Lagrangian elements is plotted. It is evident that the accuracy of LM is two orders lower than that of CM. In these cases, a linear combination of CM and LM won't be able to produce the desired HOM. Consequently, there still lacks simple, general and straightforward ways for the construction of HOM for arbitrary order elements, even in the 1D case.

As for multidimensional cases, the construction of HOM becomes much more involved and most existing works focus on 2D lower order elements. A typical example is the HOM for the square bilinear element with length h, which takes the following form [21]:

$$\begin{aligned}\boldsymbol{M}^{eh} &= \frac{3}{4}\boldsymbol{M}^{ec} + \frac{1}{4}\boldsymbol{M}^{el} \\ &= \frac{3}{4}\times\frac{h^2}{36}\begin{bmatrix}4&2&1&2\\2&4&2&1\\1&2&4&2\\2&1&2&4\end{bmatrix} \\ &\quad + \frac{1}{4}\times\frac{h^2}{4}\begin{bmatrix}1&0&0&0\\0&1&0&0\\0&0&1&0\\0&0&0&1\end{bmatrix} \\ &= \frac{h^2}{48}\begin{bmatrix}7&2&1&2\\2&7&2&1\\1&2&7&2\\2&1&2&7\end{bmatrix}\end{aligned} \tag{15}$$

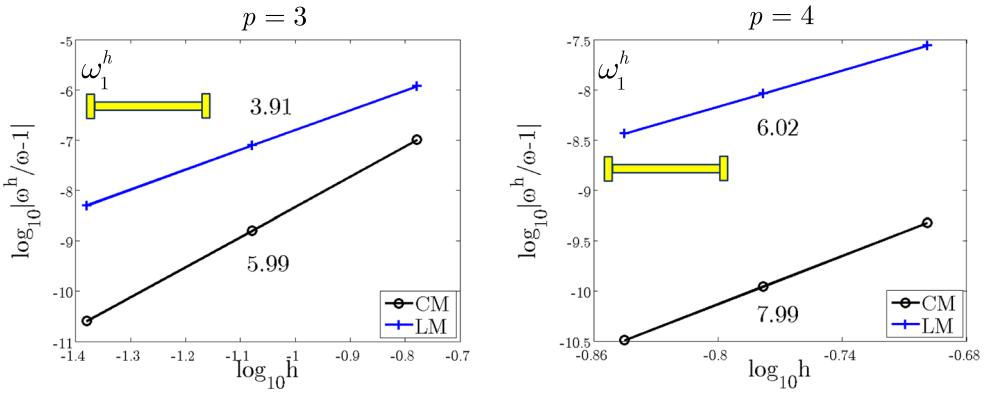

Fig. 1 Comparison of the fundamental frequency convergence for the fixed-fixed rod problem using standard cubic and quartic Lagrangian elements

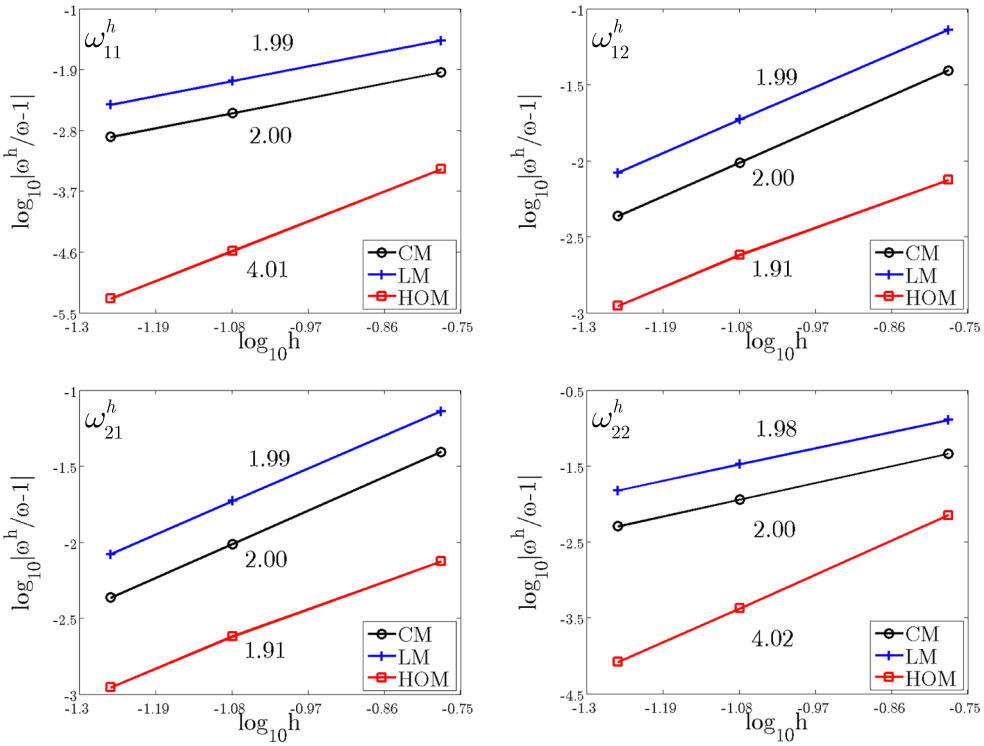

Fig. 2 Convergence comparison of the first four frequencies for the square membrane problem using HOM in Eq. (15)

With the HOM of Eq. (15), the convergence of the first four frequencies for a square membrane with fixed boundary condition are depicted in Fig. 2, where CM and LM are also included for comparison purposes. It can be seen that this HOM only elevates the convergence rates for certain frequencies, i.e., ω_{11}^h and ω_{22}^h in this example. Thus the superconvergence of this HOM shows an undesirable strong wave propagation direction dependence. One remedy for this issue is to introduce a wave propagation direction dependent optimal mass combination parameter [38,39], which however needs to be worked out on a case-by-case basis and is not computationally efficient.

On the other hand, an important observation by Hughes and Tezduyar [40] is that the 1D HOM in Eq. (13) can be obtained using the quadrature rule with integration points $\xi_{1,2} = \pm\sqrt{2/3}$ and weights $\varpi_1 = \varpi_2 = 1$:

$$\boldsymbol{M}^{eh} = \int_{x_1^e}^{x_2^e} \boldsymbol{N}^T \boldsymbol{N} dx = \frac{h}{2}\left[\boldsymbol{N}^T\left(-\sqrt{\frac{2}{3}}\right)\boldsymbol{N}\left(-\sqrt{\frac{2}{3}}\right) + \boldsymbol{N}^T\left(\sqrt{\frac{2}{3}}\right)\boldsymbol{N}\left(\sqrt{\frac{2}{3}}\right)\right] \tag{16}$$

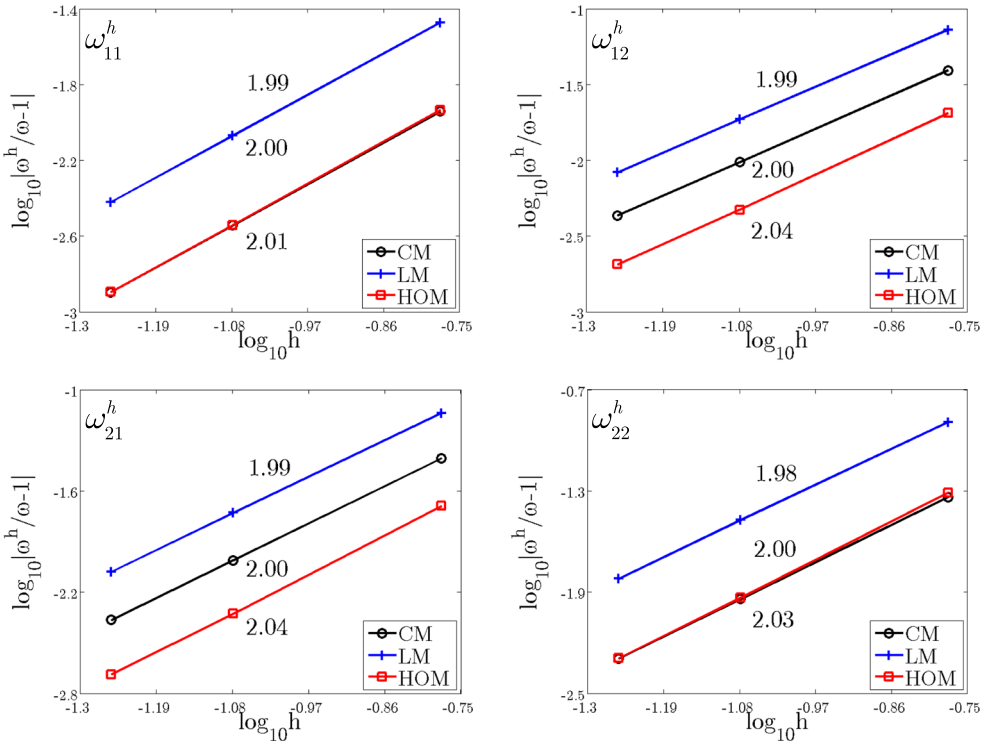

Fig. 3 Convergence comparison of the first four frequencies for the square membrane problem using the mass matrix in Eq. (17)

where $\boldsymbol{N} = \{\, N_1(\xi)\ N_2(\xi)\,\} = \{\, 1-\xi\ \ 1+\xi\,\}/2$. Conceptually, this quadrature rule would allow a straightforward tensor product extension to multidimensional formulations. Unfortunately, this direct extension does not give a 2D HOM. A straightforward calculation using the 2D tensor product version of the quadrature rule in Eq. (16) gives the following mass matrix for a square element:

$$\bar{\boldsymbol{M}}^{eh} = \frac{h^2}{144}\begin{bmatrix} 25 & 5 & 1 & 5 \\ 5 & 25 & 5 & 1 \\ 1 & 5 & 25 & 5 \\ 5 & 1 & 5 & 25 \end{bmatrix} \tag{17}$$

Based upon this postulated higher mass matrix $\bar{\boldsymbol{M}}^{eh}$, the convergence of the first four frequencies for a square membrane with fixed boundary is shown in Fig. 3. Clearly, this quadrature-based generalization of 1D HOM to 2D case does not produce the desired superconvergence with 4th order accurate frequencies. We will come back to this point later to investigate the reason behind this phenomena.

In summary, the previous discussions indicate the following typical issues associated with the higher order mass matrix formulation: (1) Are there simple and general methods to construct 1D HOM for arbitrary order elements? (2) Are there simple and unified superconvergent formulations for multidimensional arbitrary order elements? (3) Can the wave propagation direction dependence issue in the superconvergent frequency computation be eliminated by a concise formulation? In this work, we try to address these issues through a unified quadrature-based formulation.

4 Unified formulation of 1D higher order mass matrices

4.1 General formulation

We first present a unified formulation for 1D higher order mass matrices. As mentioned earlier, the lumped mass matrices of Lagrangian cubic and quartic elements with equal nodal spacing do not provide an equal accuracy order as their consistent counterparts. Alternatively, here we employ the Lobatto elements which take the roots of the following equation as the elemental interpolation points [7]:

$$(1-\xi^2)P_n'(\xi) = 0 \tag{18}$$

with $P_n(\xi)$ being the nth order Legendre polynomial:

$$P_n(\xi) = \frac{1}{2^n n!}\frac{d^n}{d\xi^n}[(\xi^2-1)^n],\ \ \xi \in [-1,\ 1] \tag{19}$$

For convenience of presentation, the nodal locations of the linear, quadratic, cubic and quartic Lobatto elements are illustrated in Fig. 4. It is seen that nodal locations of linear

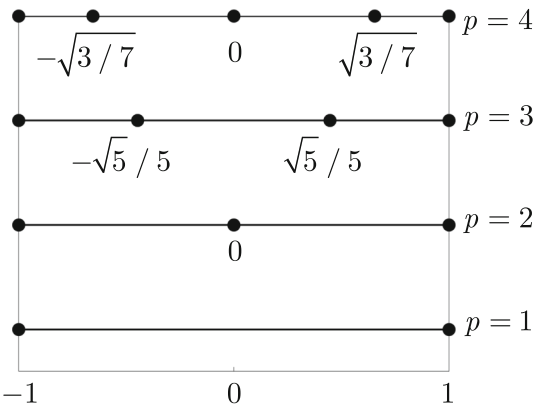

Fig. 4 Nodal locations of the linear, quadratic, cubic and quartic Lobatto elements

and quadratic Lobatto elements coincide with the standard Lagrangian elements, while non-uniform node distributions occur for the higher order elements such as cubic and quartic Lobatto elements.

The shape functions of Lobatto elements are obtained through the Lagrangian interpolation based upon the nodal locations in Fig. 4. The shape functions of the linear and quadratic Lobatto elements are identical to their Lagrangian counterparts and the shape functions of cubic and quartic elements are:

$$\begin{cases} N_1(\xi) = -\frac{5}{8}\left(\xi + \frac{\sqrt{5}}{5}\right)\left(\xi - \frac{\sqrt{5}}{5}\right)(\xi - 1) \\ N_2(\xi) = \frac{5\sqrt{5}}{8}(\xi + 1)\left(\xi - \frac{\sqrt{5}}{5}\right)(\xi - 1) \\ N_3(\xi) = -\frac{5\sqrt{5}}{8}(\xi + 1)\left(\xi + \frac{\sqrt{5}}{5}\right)(\xi - 1) \\ N_4(\xi) = \frac{5}{8}(\xi + 1)\left(\xi + \frac{\sqrt{5}}{5}\right)\left(\xi - \frac{\sqrt{5}}{5}\right) \end{cases} \tag{20}$$

$$\begin{cases} N_1(\xi) = \frac{7}{8}\xi\left(\xi + \sqrt{\frac{3}{7}}\right)\left(\xi - \sqrt{\frac{3}{7}}\right)(\xi - 1) \\ N_2(\xi) = -\frac{49}{24}\xi(\xi + 1)\left(\xi - \sqrt{\frac{3}{7}}\right)(\xi - 1) \\ N_3(\xi) = \frac{7}{3}(\xi + 1)\left(\xi + \sqrt{\frac{3}{7}}\right)\left(\xi - \sqrt{\frac{3}{7}}\right)(\xi - 1) \\ N_4(\xi) = -\frac{49}{24}\xi(\xi + 1)\left(\xi + \sqrt{\frac{3}{7}}\right)(\xi - 1) \\ N_5(\xi) = \frac{7}{8}\xi(\xi + 1)\left(\xi + \sqrt{\frac{3}{7}}\right)\left(\xi - \sqrt{\frac{3}{7}}\right) \end{cases} \tag{21}$$

The cubic and quartic shape functions defined in Eqs. (20) and (21) are drawn in Fig. 5, where one unique property for the Lobatto elements is that their shape functions arrive at the maximum values of 1 always at the nodes, while the maximum values and nodes are different for some interior points

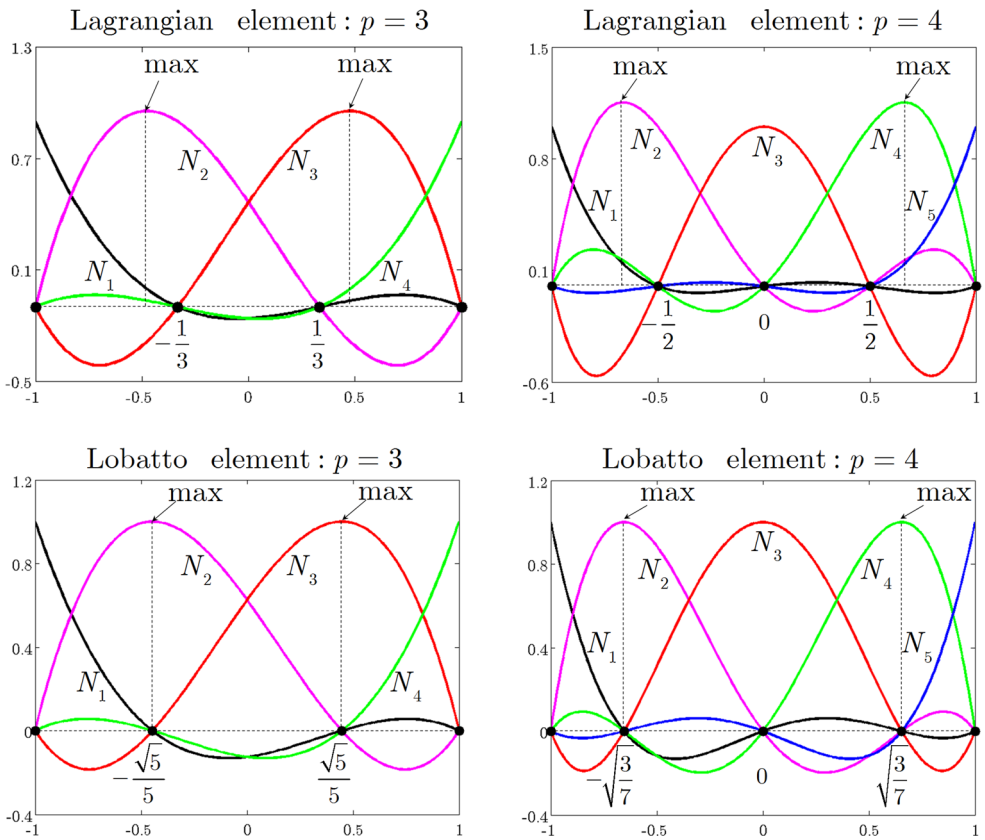

Fig. 5 Comparison of the shape functions of the cubic and quartic Lagrangian and Lobatto elements

of the standard Lagrangian elements. Roughly speaking, the shape functions of Lobatto elements are less oscillatory than those of Lagrangian elements with equally spaced nodes.

For convenience of theoretical development, the explicit expressions of consistent mass matrices for the cubic and quartic Lobatto elements are given as follows:

$$\boldsymbol{M}^{ec} = \frac{h}{84}\begin{bmatrix} 6 & \sqrt{5} & -\sqrt{5} & 1 \\ \sqrt{5} & 30 & 5 & -\sqrt{5} \\ -\sqrt{5} & 5 & 30 & \sqrt{5} \\ 1 & -\sqrt{5} & \sqrt{5} & 6 \end{bmatrix} \tag{22}$$

$$\boldsymbol{M}^{ec} = \frac{h}{1620}\begin{bmatrix} 72 & 21 & -24 & 21 & -9 \\ 21 & 392 & 56 & -49 & 21 \\ -24 & 56 & 512 & 56 & -24 \\ 21 & -49 & 56 & 392 & 21 \\ -9 & 21 & -24 & 21 & 72 \end{bmatrix} \tag{23}$$

Their lumped mass counterparts can be obtained simply via the row-sum method. We will see later that both consistent and lumped mass matrices of Lobatto elements give a frequency accuracy of $O(h^{2p})$ for the wave equations.

Based upon the family of Lobatto elements, we propose the following mass template to construct 1D higher order mass matrices:

$$\begin{cases} M^{e\alpha}_{aa} = \frac{1}{\alpha}\left(\alpha \sum\limits_{b} M^{ec}_{ab} - \sum\limits_{b\neq a} M^{ec}_{ab}\right) \\ M^{e\alpha}_{ab} = \frac{1}{\alpha} M^{ec}_{ab} \quad a \neq b \end{cases} ;\ a,b = 1, 2, \ldots, n_{en} \tag{24}$$

where α is a parameter to be optimized and here we refer $\boldsymbol{M}^{e\alpha}$ as the α mass matrix. Clearly, by construction $\boldsymbol{M}^{e\alpha}$ preserves the total mass of the consistent mass matrix. Next we will show the optimal choice of α, i.e., α_{opt}, such as the 1D higher order mass matrix $\boldsymbol{M}^{eh} = \boldsymbol{M}^{e\alpha}(\alpha_{opt})$.

4.2 Linear element

For a two-node linear element with $p = 1$, following Eq. (24), the α mass matrix $\boldsymbol{M}^{e\alpha}$ corresponding to the consistent mass matrix in Eq. (13) is:

$$\boldsymbol{M}^{e\alpha} = \frac{h}{6\alpha}\begin{bmatrix} 3\alpha - 1 & 1 \\ 1 & 3\alpha - 1 \end{bmatrix} \tag{25}$$

The stiffness matrix $\boldsymbol{K}^e$ for the linear element is:

$$\boldsymbol{K}^e = \frac{c^2}{h}\begin{bmatrix} 1 & -1 \\ -1 & 1 \end{bmatrix} \tag{26}$$

Thus the stencil equation associated with a typical node x_A corresponding to Eq. (6) is:

$$\frac{h}{6\alpha}\left[\ddot{d}_{A-1} + (6\alpha - 2)\ddot{d}_A + \ddot{d}_{A+1}\right] + \frac{c^2}{h}\left(-d_{A-1} + 2d_A - d_{A+1}\right) = 0 \tag{27}$$

where the uppercase subscript "A" denotes the global node numbering.

Consider a harmonic representation of the nodal degree of freedom d_A as:

$$\begin{cases} d_A(t) = d_0 \exp[\iota(kx_A - \omega^h t)] \\ \ddot{d}_A(t) = -(\omega^h)^2 d_0 \exp[\iota(kx_A - \omega^h t)] \end{cases} \tag{28}$$

Substituting Eqs. (28) into (27) yields:

$$-(\omega^h)^2[\cos kh + (3\alpha - 1)] = \frac{6c^2\alpha}{h^2}(\cos kh - 1) \tag{29}$$

Then the semi-discrete frequency ω^h is obtained as:

$$\frac{\omega^h}{\omega} = \frac{1}{kh}\sqrt{\frac{6\alpha(1 - \cos kh)}{\cos kh + (3\alpha - 1)}} \tag{30}$$

where $\omega = kc$, as shown in Eq. (3). Further invoking the Taylor's expansion, Eq. (30) can be rephrased as:

$$\frac{\omega^h}{\omega} \approx \sqrt{\frac{\vartheta}{\psi}} \approx 1 + \frac{\vartheta - \psi}{2\vartheta} \tag{31}$$

with

$$\begin{cases} \vartheta = 6\alpha - \frac{1}{2}\alpha(kh)^2 + \frac{1}{60}\alpha(kh)^4 \\ \psi = 6\alpha - (kh)^2 + \frac{1}{12}(kh)^4 \end{cases} \tag{32}$$

By Eqs. (31), (32) reduces to:

$$\frac{\omega^h}{\omega} \approx 1 + \frac{2 - \alpha}{24\alpha}(kh)^2 + O(kh)^4 \tag{33}$$

Obviously, choosing $\alpha = \alpha_{opt} = 2 = p + 1$ in Eq. (33) gives a 4th order accurate frequency, and this corresponds to the following higher order mass matrix:

$$\boldsymbol{M}^{eh} = \boldsymbol{M}^{e\alpha}(\alpha_{opt}) = \frac{h}{12}\begin{bmatrix} 5 & 1 \\ 1 & 5 \end{bmatrix} \tag{34}$$

Thus the proposed α mass matrix with an optimal parameter $\alpha_{opt} = 2 = p + 1$ exactly recovers the original higher order mass matrix of Eq. (13).

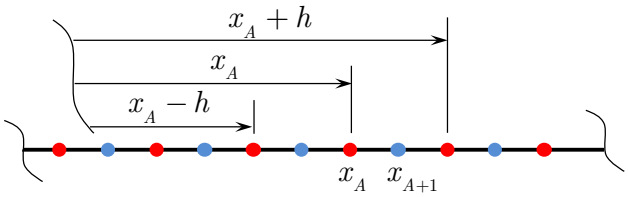

Fig. 6 Nodal distribution and influence domains of quadratic elements

4.3 Quadratic element

With aid of the consistent mass matrix in Eq. (14) for a quadratic element, the α mass matrix of Eq. (24) becomes:

$$\boldsymbol{M}^{e\alpha} = \frac{h}{30\alpha}\begin{bmatrix} 5\alpha-1 & 2 & -1 \\ 2 & 20\alpha-4 & 2 \\ -1 & 2 & 5\alpha-1 \end{bmatrix} \tag{35}$$

In the meantime, the stiffness matrix $\boldsymbol{K}^e$ is given by:

$$\boldsymbol{K}^e = \frac{c^2}{3h}\begin{bmatrix} 7 & -8 & 1 \\ -8 & 16 & -8 \\ 1 & -8 & 7 \end{bmatrix} \tag{36}$$

While for the three-node quadratic element, as shown in Fig. 6, it is noted that the shape functions and their influence domains are different for the elemental interior node x_A and boundary node x_{A+1}, thus the stencil equations are attached with two neighboring nodes x_A and x_{A+1} [18]:

$$\begin{cases} \frac{h}{10\alpha}[-\ddot{d}_{A-2} + 2\ddot{d}_{A-1} + (10\alpha-2)\ddot{d}_A + 2\ddot{d}_{A+1} - \ddot{d}_{A+2}] \\ + \frac{c^2}{h}[d_{A-2} - 8d_{A-1} + 14d_A - 8d_{A+1} + d_{A+2}] = 0 \\ \frac{h}{10\alpha}[\ddot{d}_A + (10\alpha-2)\ddot{d}_{A+1} + \ddot{d}_{A+2}] + \frac{c^2}{h}[-4d_A \\ + 8d_{A+1} - 4d_{A+2}] = 0 \end{cases} \tag{37}$$

Assuming harmonic forms for both d_A and d_{A+1} gives:

$$\begin{cases} d_A(t) = d_{01}\exp[\iota(kx_A - \omega^h t)] \\ d_{A+1}(t) = d_{02}\exp[\iota(kx_{A+1} - \omega^h t)] \end{cases} \tag{38}$$

$$\begin{cases} \ddot{d}_A(t) = -(\omega^h)^2 d_{01}\exp[\iota(kx_A - \omega^h t)] \\ \ddot{d}_{A+1}(t) = -(\omega^h)^2 d_{02}\exp[\iota(kx_{A+1} - \omega^h t)] \end{cases} \tag{39}$$

where d_{01} and d_{02} are two wave amplitudes. Plugging Eqs. (38) and (39) into (37) gives:

$$\begin{bmatrix} -(\omega^h h)^2\cos\frac{kh}{2} - 40c^2\alpha\cos\frac{kh}{2} & -(\omega^h h)^2(5\alpha-1) + 40c^2\alpha \\ (\omega^h h)^2\cos kh - (\omega^h h)^2(5\alpha-1) & -2(\omega^h h)^2\cos\frac{kh}{2} - 80c^2\alpha\cos\frac{kh}{2} \\ +10c^2\alpha\cos kh + 70c^2\alpha & \end{bmatrix} \times \begin{Bmatrix} d_{01} \\ d_{02} \end{Bmatrix} = 0 \tag{40}$$

Clearly Eq. (40) implies the vanishing of the determinant of the coefficient matrix, i.e.,

$$g_4(\omega^h)^4 + g_2(\omega^h)^2 + g_0 = 0 \tag{41}$$

with

$$\begin{cases} g_4 = -2h^4\cos^2(\frac{kh}{2}) - 5\alpha h^4\cos(kh) + 25\alpha^2 h^4 \\ \quad + h^4\cos(kh) - 10\alpha h^4 + h^4 \\ g_2 = -160c^2\alpha h^2\cos^2(\frac{kh}{2}) - 50c^2\alpha^2 h^2\cos(kh) \\ \quad + 50c^2\alpha h^2\cos(kh) - 550c^2\alpha^2 h^2 + 110c^2\alpha h^2 \\ g_0 = -3200c^4\alpha^2\cos^2(\frac{kh}{2}) + 400c^4\alpha^2\cos(kh) + 2800c^4\alpha^2 \end{cases} \tag{42}$$

Then $(\omega^h)^2$ can be obtained from Eq. (41) as:

$$(\omega^h)^2 = \frac{-g_2 - \sqrt{g_2^2 - 4g_0 g_4}}{2g_4} \tag{43}$$

Subsequently through the employment of Taylor's expansion, Eq. (43) becomes:

$$(\omega^h)^2 \approx \frac{c^2\left[(-30\alpha + 50\alpha^2)(kh)^2 + 5\alpha(kh)^4 - \frac{1}{144}(5\alpha^2 + 42\alpha + 9)(kh)^6\right]}{50\alpha^2 h^2 - 30\alpha h^2 + 5\alpha h^2(kh)^2 - \frac{5}{12}\alpha h^2(kh)^4} \tag{44}$$

Note that $\omega = kc$, we can also reach the form of Eq. (31) with the following parameters:

$$\begin{cases} \vartheta = (50\alpha^2 - 30\alpha) + 5\alpha(kh)^2 - \frac{1}{144}(5\alpha^2 + 42\alpha + 9)(kh)^4 \\ \psi = (50\alpha^2 - 30\alpha) + 5\alpha(kh)^2 - \frac{5}{12}\alpha(kh)^4 \end{cases} \tag{45}$$

Thus the frequency error is finally derived as:

$$\frac{\omega^h}{\omega} \approx 1 + \frac{-5\alpha^2 + 18\alpha - 9}{14400\alpha^2 - 8640\alpha}(kh)^4 + O(kh)^6 \tag{46}$$

It is clear now that if the following relationship holds:

$$-5\alpha^2 + 18\alpha - 9 = 0 \;\Rightarrow\; \alpha_{opt} = 3 = p + 1 \tag{47}$$

we will have a 6th order accuracy that is associated with the following higher order mass matrix:

$$\boldsymbol{M}^{eh} = \boldsymbol{M}^{e\alpha}(\alpha_{opt} = 3) = \frac{h}{90}\begin{bmatrix} 14 & 2 & -1 \\ 2 & 56 & 2 \\ -1 & 2 & 14 \end{bmatrix} \tag{48}$$

Once again the proposed method produces the higher order mass matrix of Eq. (14) if we select $\alpha_{opt} = p + 1$, where p is the order of the shape functions.

4.4 Cubic and quartic elements

It can be seen that the derivation of higher order mass matrix for quadratic element is already very involved, thus it would be extremely complicated to carry out the derivations of higher order mass matrices for cubic and quartic elements. However, the detailed derivations of linear and quadratic elements have demonstrated that the proposed α mass matrix in Eq. (24) directly yields the desired higher order mass matrix when $\alpha_{opt} = p + 1$. Consequently in this sub-section, the higher order mass matrices for cubic and quartic elements are established using the proposed α mass matrix, and their effectiveness will be validated shortly by benchmark examples.

For the cubic element with $p = 3$, its consistent mass matrix is given by Eq. (22) and the corresponding α mass matrix in Eq. (24) takes the following form:

$$\boldsymbol{M}^{e\alpha} = \frac{h}{84\alpha}\begin{bmatrix} 7\alpha-1 & \sqrt{5} & -\sqrt{5} & 1 \\ \sqrt{5} & 35\alpha-5 & 5 & -\sqrt{5} \\ -\sqrt{5} & 5 & 35\alpha-5 & \sqrt{5} \\ 1 & -\sqrt{5} & \sqrt{5} & 7\alpha-1 \end{bmatrix} \tag{49}$$

Further choosing $\alpha = \alpha_{opt} = p + 1 = 4$ in Eq. (49) yields the cubic higher order mass matrix:

$$\boldsymbol{M}^{eh} = \boldsymbol{M}^{e\alpha}(\alpha_{opt} = 4) = \frac{h}{336}\begin{bmatrix} 27 & \sqrt{5} & -\sqrt{5} & 1 \\ \sqrt{5} & 135 & 5 & -\sqrt{5} \\ -\sqrt{5} & 5 & 135 & \sqrt{5} \\ 1 & -\sqrt{5} & \sqrt{5} & 27 \end{bmatrix} \tag{50}$$

A similar argument for the quartic element with $p = 4$ leads to the following α mass matrix and higher order mass matrix:

$$\boldsymbol{M}^{e\alpha} = \frac{h}{1620\alpha} \times \begin{bmatrix} 81\alpha-9 & 21 & -24 & 21 & -9 \\ 21 & 441\alpha-49 & 56 & -49 & 21 \\ -24 & 56 & 576\alpha-64 & 56 & -24 \\ 21 & -49 & 56 & 441\alpha-49 & 21 \\ -9 & 21 & -24 & 21 & 81\alpha-9 \end{bmatrix} \tag{51}$$

$$\boldsymbol{M}^{eh} = \boldsymbol{M}^{e\alpha}(\alpha_{opt} = 5) = \frac{h}{8100}\begin{bmatrix} 396 & 21 & -24 & 21 & -9 \\ 21 & 2156 & 56 & -49 & 21 \\ -24 & 56 & 2816 & 56 & -24 \\ 21 & -49 & 56 & 2156 & 21 \\ -9 & 21 & -24 & 21 & 396 \end{bmatrix} \tag{52}$$

The higher order mass matrices of cubic and quartic elements are expected to produce 8th and 10th order accurate frequencies, respectively.

4.5 Numerical examinations

In this sub-section, we take the free vibration analysis of an elastic rod to assess the present unified 1D higher order mass matrix formulation. Three types of boundary conditions, i.e., free-free, fixed-free and fixed-fixed, are considered and the analytical frequencies are [42]:

$$\omega_i = \begin{cases} ic\pi/L & \text{fixed-fixed or free-free rod} \\ (2i-1)c\pi/(2L) & \text{fixed-free rod} \end{cases} \tag{53}$$

where L is the rod length, $c = \sqrt{E/\rho}$ is the wave speed, E is Young's modulus and ρ is the material density. Without loss of generality, unit values are set for all the geometry and material properties.

Particular emphasis is placed on the higher order mass matrices of cubic and quartic elements since the linear and quadratic higher order mass matrices recover the existing ones [21]. Figures 7 and 8 show the frequency convergence for the elastic rod problems using various mass matrices of the cubic and quartic Lobatto elements, respectively. The results clearly prove that for both cubic and quartic Lobatto elements, the proposed HOM yields an expected superconvergence with 8th and 10th orders of accuracy, while 6th and 8th order accurate frequencies are obtained by CM and LM.

5 Multidimensional unified superconvergent formulations

In this section, a unified superconvergent formulation is presented for multidimensional problems based on certain quadrature rules which are simultaneously employed to integrate both the mass and stiffness matrices. The superconvergent quadrature rules are rationally derived through optimizing the frequency accuracy. More importantly, it is shown that these quadrature rules happen to be the exact integration rules for the 1D higher order mass matrices presented in Sect. 3.

5.1 Quadrature-based superconvergent formulation for 2D bilinear element

Consider a uniform discretization with rectangular bilinear elements as shown in Fig. 9, the element has length h_x and height h_y, and the Jacobian J for this element is $J = h_x h_y/4$. If we use a two-point quadrature rule, i.e., integration points

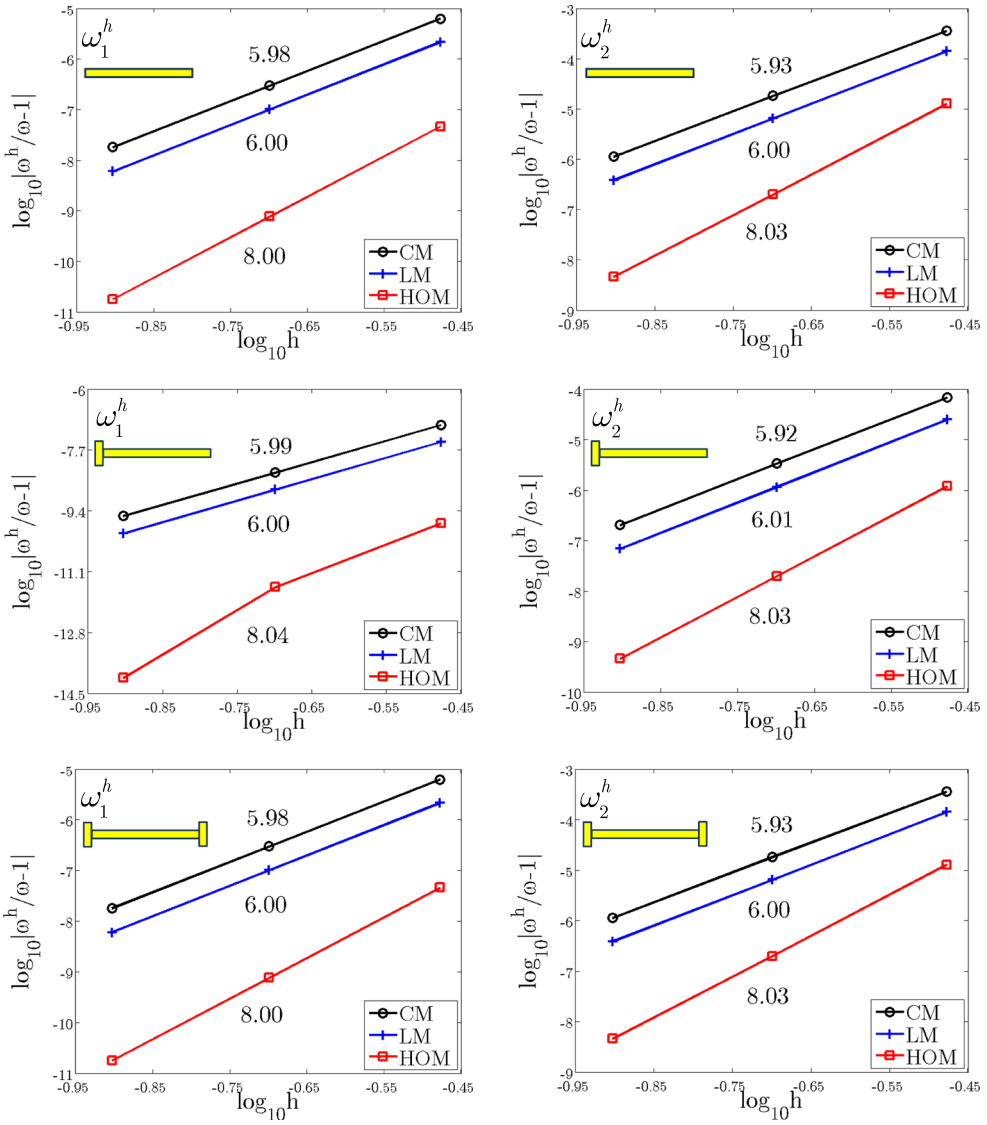

Fig. 7 Convergence comparison of the first two frequencies for the elastic rod problems using various mass matrices of cubic Lobatto element

$\pm\tilde{\xi}$ and weights $\varpi_1 = \varpi_2 = 1$, then the discrete mass matrix $\tilde{\boldsymbol{M}}^e$ becomes:

$$\tilde{\boldsymbol{M}}^e = \frac{h_x h_y}{4}\sum_{i,j=1}^{2} \boldsymbol{N}^T(\tilde{\xi}_i,\tilde{\xi}_j)\boldsymbol{N}(\tilde{\xi}_i,\tilde{\xi}_j)\varpi_i\varpi_j = \frac{h_x h_y}{16}\begin{bmatrix} (\tilde{\xi}^2+1)^2 & (1-\tilde{\xi}^4) & (1-\tilde{\xi}^2)^2 & (1-\tilde{\xi}^4) \\ (1-\tilde{\xi}^4) & (\tilde{\xi}^2+1)^2 & (1-\tilde{\xi}^4) & (1-\tilde{\xi}^2)^2 \\ (1-\tilde{\xi}^2)^2 & (1-\tilde{\xi}^4) & (\tilde{\xi}^2+1)^2 & (1-\tilde{\xi}^4) \\ (1-\tilde{\xi}^4) & (1-\tilde{\xi}^2)^2 & (1-\tilde{\xi}^4) & (\tilde{\xi}^2+1)^2 \end{bmatrix} \tag{54}$$

where the row vector $\boldsymbol{N}$ contains the four standard bilinear shape functions [1]. Similarly, the discrete stiffness matrix $\tilde{\boldsymbol{K}}^e$ is given by:

$$\tilde{\boldsymbol{K}}^e = \frac{c^2 h_x h_y}{4}\sum_{i,j=1}^{2} \boldsymbol{B}^T(\tilde{\xi}_i,\tilde{\xi}_j)\boldsymbol{B}(\tilde{\xi}_i,\tilde{\xi}_j)\varpi_i\varpi_j = \frac{c^2 h_x h_y}{4}\begin{bmatrix} \tilde{\boldsymbol{K}}^e_{11} & \tilde{\boldsymbol{K}}^e_{12} \\ \tilde{\boldsymbol{K}}^{eT}_{12} & \tilde{\boldsymbol{K}}^e_{22} \end{bmatrix} \tag{55}$$

where $\boldsymbol{B}$ is the gradient matrix corresponding to $\boldsymbol{N}$. The sub-matrices $\tilde{\boldsymbol{K}}^e_{ab}$'s are:

$$\tilde{\boldsymbol{K}}^e_{11} = \begin{bmatrix} \left(\frac{1}{h_x^2}+\frac{1}{h_y^2}\right)\left(1+\tilde{\xi}^2\right) & -\frac{1}{h_x^2}\left(1+\tilde{\xi}^2\right)+\frac{1}{h_y^2}\left(1-\tilde{\xi}^2\right) \\ -\frac{1}{h_x^2}\left(1+\tilde{\xi}^2\right)+\frac{1}{h_y^2}\left(1-\tilde{\xi}^2\right) & \left(\frac{1}{h_x^2}+\frac{1}{h_y^2}\right)\left(1+\tilde{\xi}^2\right) \end{bmatrix} \tag{56}$$

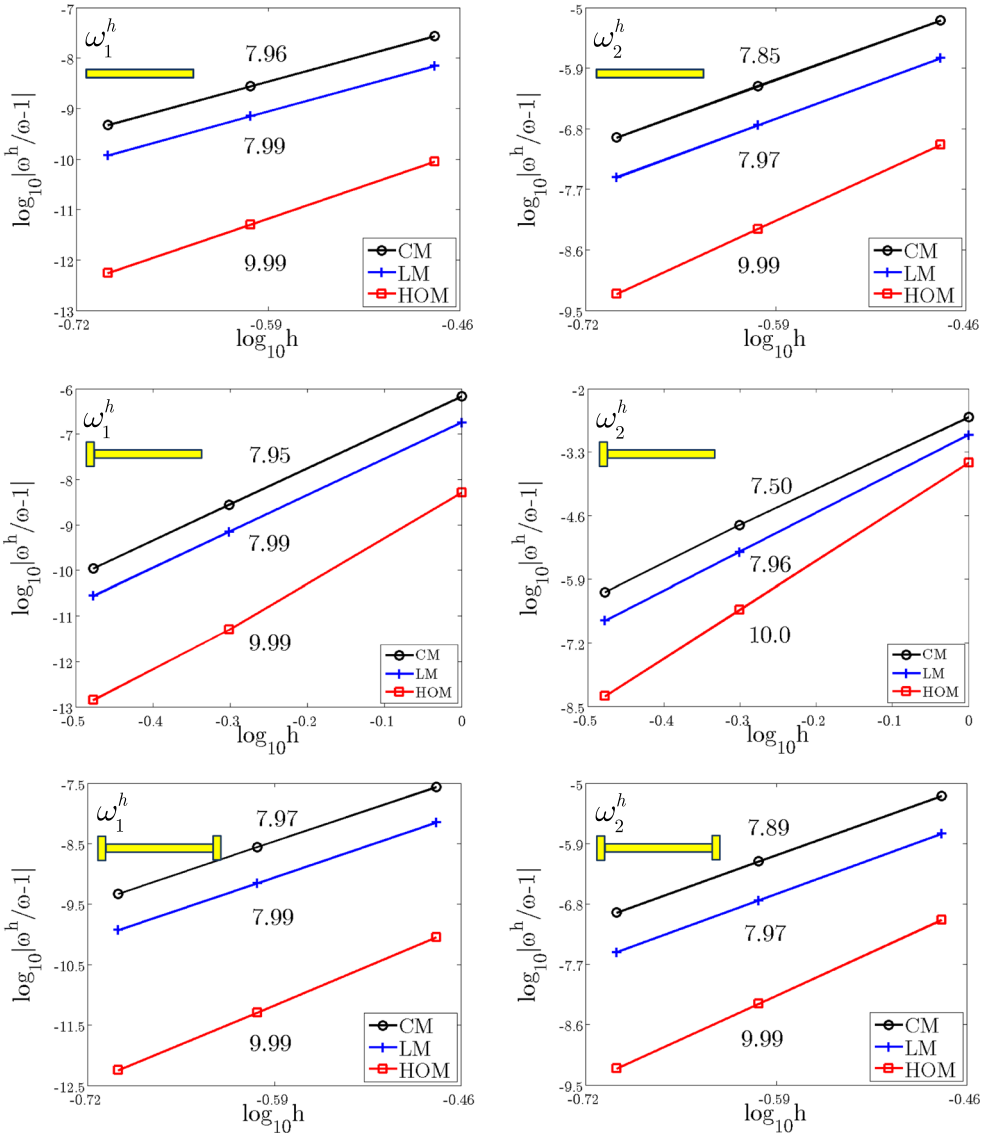

Fig. 8 Convergence comparison of the first two frequencies for the elastic rod problems using various mass matrices of quartic Lobatto element

$$\tilde{\boldsymbol{K}}_{12}^{e} = \begin{bmatrix} -\frac{1}{h_x^2}\left(1-\tilde{\xi}^2\right) - \frac{1}{h_y^2}\left(1-\tilde{\xi}^2\right) & \frac{1}{h_x^2}\left(1-\tilde{\xi}^2\right) - \frac{1}{h_y^2}\left(1+\tilde{\xi}^2\right) \\ \frac{1}{h_x^2}\left(1-\tilde{\xi}^2\right) - \frac{1}{h_y^2}\left(1+\tilde{\xi}^2\right) & -\frac{1}{h_x^2}\left(1-\tilde{\xi}^2\right) - \frac{1}{h_y^2}\left(1-\tilde{\xi}^2\right) \end{bmatrix} \tag{57}$$

$$\tilde{\boldsymbol{K}}_{22}^{e} = \begin{bmatrix} \left(\frac{1}{h_x^2}+\frac{1}{h_y^2}\right)\left(1+\tilde{\xi}^2\right) & -\frac{1}{h_x^2}\left(1+\tilde{\xi}^2\right) + \frac{1}{h_y^2}\left(1-\tilde{\xi}^2\right) \\ -\frac{1}{h_x^2}\left(1+\tilde{\xi}^2\right) + \frac{1}{h_y^2}\left(1-\tilde{\xi}^2\right) & \left(\frac{1}{h_x^2}+\frac{1}{h_y^2}\right)\left(1+\tilde{\xi}^2\right) \end{bmatrix} \tag{58}$$

For a typical node $\boldsymbol{x}_{AB}$, the discrete equation of motion of Eq. (6) reads:

$$\mathcal{H}(\ddot{d}_{AB}) + c^2\mathcal{G}(d_{AB}) = 0 \tag{59}$$

where $\mathcal{H}(\ddot{d}_{AB})$ and $\mathcal{G}(d_{AB})$ are:

$$\mathcal{H}\left(\ddot{d}_{AB}\right)=\frac{1}{16}\left[\begin{array}{l}\left(1-\tilde{\xi}^2\right)^2\ddot{d}_{(A-1)(B+1)}+2\left(1-\tilde{\xi}^4\right)\ddot{d}_{(A-1)B}+\left(1-\tilde{\xi}^2\right)^2\ddot{d}_{(A-1)(B-1)}\\+2\left(1-\tilde{\xi}^4\right)\ddot{d}_{A(B+1)}+4\left(\tilde{\xi}^2+1\right)^2\ddot{d}_{AB}+2\left(1-\tilde{\xi}^4\right)\ddot{d}_{A(B-1)}\\+\left(1-\tilde{\xi}^2\right)^2\ddot{d}_{(A+1)(B+1)}+2\left(1-\tilde{\xi}^4\right)\ddot{d}_{(A+1)B}\\+\left(1-\tilde{\xi}^2\right)^2\ddot{d}_{(A+1)(B-1)}\end{array}\right] \tag{60}$$

$$\mathcal{G}(d_{AB})=\frac{1}{4}\left\{\begin{array}{l}-\left(\frac{1}{h_x^2}+\frac{1}{h_y^2}\right)\left(1-\tilde{\xi}^2\right)d_{(A-1)(B+1)}-\left[\frac{2}{h_x^2}\left(1+\tilde{\xi}^2\right)-\frac{2}{h_y^2}\left(1-\tilde{\xi}^2\right)\right]d_{(A-1)B}\\-\left(\frac{1}{h_x^2}+\frac{1}{h_y^2}\right)\left(1-\tilde{\xi}^2\right)d_{(A-1)(B-1)}+\left[\frac{2}{h_x^2}\left(1-\tilde{\xi}^2\right)-\frac{2}{h_y^2}\left(1+\tilde{\xi}^2\right)\right]d_{A(B+1)}\\+\left(\frac{4}{h_x^2}+\frac{4}{h_y^2}\right)\left(\tilde{\xi}^2+1\right)d_{AB}+\left[\frac{2}{h_x^2}\left(1-\tilde{\xi}^2\right)-\frac{2}{h_y^2}\left(1+\tilde{\xi}^2\right)\right]d_{A(B-1)}\\-\left(\frac{1}{h_x^2}+\frac{1}{h_y^2}\right)\left(1-\tilde{\xi}^2\right)d_{(A+1)(B+1)}-\left[\frac{2}{h_x^2}\left(1+\tilde{\xi}^2\right)-\frac{2}{h_y^2}\left(1-\tilde{\xi}^2\right)\right]d_{(A+1)B}\\+\left(-\frac{1}{h_x^2}-\frac{1}{h_y^2}\right)\left(1-\tilde{\xi}^2\right)d_{(A+1)(B-1)}\end{array}\right\} \tag{61}$$

Following the similar procedure as 1D analysis, d_{AB} takes the following form:

$$\begin{cases}d_{AB}(t)=d_0\exp[\iota(k_xx_A+k_yy_B-\omega^ht)]\\ \ddot{d}_{AB}(t)=-(\omega^h)^2d_0\exp[\iota(k_xx_A+k_yy_B-\omega^ht)]\end{cases} \tag{62}$$

For convenience of presentation, assume $h_y=sh_x=sh$ and introduce the wave propagation angle θ as shown in Fig. 9:

$$k_x=k\cos\theta,\quad k_y=k\sin\theta \tag{63}$$

Then bringing Eqs. (62) into (59) gives:

$$-(\omega^h)^2\mathcal{S}+c^2\mathcal{T}=0 \tag{64}$$

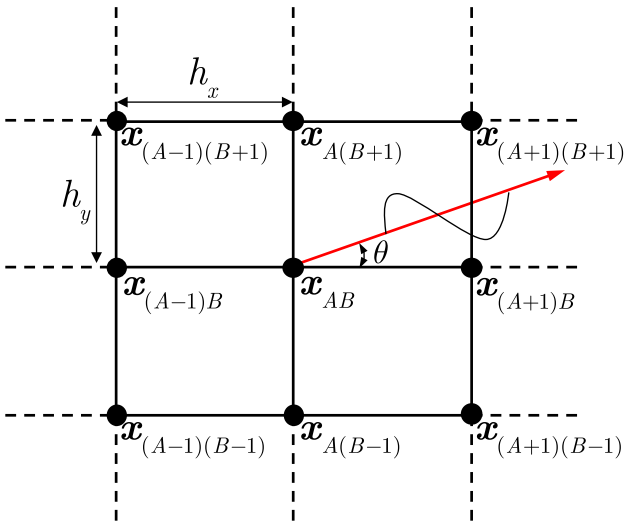

Fig. 9 A finite element mesh with bilinear rectangular elements

with

$$\begin{aligned}\mathcal{S}=&\frac{1}{2}(1-\tilde{\xi}^2)^2\cos(-kh\cos\theta+skh\sin\theta)\\&+(1-\tilde{\xi}^4)\cos(-kh\cos\theta)\\&+\frac{1}{2}(1-\tilde{\xi}^2)^2\cos(-kh\cos\theta-skh\sin\theta)\\&+(1-\tilde{\xi}^4)\cos(skh\sin\theta)\\&+(\tilde{\xi}^2+1)^2\end{aligned} \tag{65}$$

$$\begin{aligned}\mathcal{T}=&\left[-\frac{2}{h^2}(1-\tilde{\xi}^2)-\frac{2}{s^2h^2}(1-\tilde{\xi}^2)\right]\\&\times\cos\left[kh(-\cos\theta+s\sin\theta)\right]\\&+\left[-\frac{4}{h^2}(1+\tilde{\xi}^2)+\frac{4}{s^2h^2}(1-\tilde{\xi}^2)\right]\cos(-kh\cos\theta)\\&+\left[-\frac{2}{h^2}(1-\tilde{\xi}^2)-\frac{2}{s^2h^2}(1-\tilde{\xi}^2)\right]\\&\times\cos\left[kh(-\cos\theta-s\sin\theta)\right]\\&+\left[\frac{4}{h^2}(1-\tilde{\xi}^2)-\frac{4}{s^2h^2}(1+\tilde{\xi}^2)\right]\cos(skh\sin\theta)\\&+\left[4\times\left(\frac{1}{h^2}+\frac{1}{s^2h^2}\right)(1+\tilde{\xi}^2)\right]\end{aligned} \tag{66}$$

Thus we arrive at:

$$\omega^h=c\sqrt{\frac{\mathcal{T}}{\mathcal{S}}} \tag{67}$$

By performing Taylor's expansions on $\mathcal{T}$ and $\mathcal{S}$, Eq. (67) can be recast into the form of Eq. (31), where at this time ϑ and ψ are given by:

$$\vartheta = 4 + \left[-\tfrac{1}{3}\cos^4\theta - \tfrac{1}{3}s^2\sin^4\theta + \cos^2\theta\sin^2\theta(s^2\tilde{\xi}^2 + \tilde{\xi}^2 - s^2 - 1)\right](kh)^2 + \left[\begin{array}{l} \tfrac{1}{90}\cos^6\theta + \tfrac{1}{90}\alpha^4\sin^6\theta + \cos^2\theta\sin^2\theta\times \\ \left(-\tfrac{1}{12}s^2\tilde{\xi}^2 + \tfrac{1}{12}s^2 + \tfrac{1}{12}s^4\sin^2\theta + \tfrac{1}{12}\cos^2\theta \right. \\ \left. -\tfrac{1}{12}\tilde{\xi}^2\cos^2\theta - \tfrac{1}{12}s^4\tilde{\xi}^2\sin^2\theta\right) \end{array}\right](kh)^4 \quad (68)$$

$$\psi = 4 + \left[\begin{array}{l} (\tilde{\xi}^2 - 1)\cos^4\theta + (\tilde{\xi}^2 - 1)s^2\sin^4\theta \\ +\cos^2\theta\sin^2\theta(s^2\tilde{\xi}^2 + \tilde{\xi}^2 - s^2 - 1) \end{array}\right](kh)^2 + \left[\begin{array}{l} \left(\tfrac{1}{12} - \tfrac{1}{12}\tilde{\xi}^2\right)\cos^6\theta + (\tfrac{1}{12}s^4 - \tfrac{1}{12}s^4\tilde{\xi}^2)\sin^6\theta \\ +\sin^2\theta\cos^2\theta\times\left(\tfrac{1}{12}s^4\sin^2\theta - \tfrac{1}{12}s^4\tilde{\xi}^2\sin^2\theta + \right. \\ \left. \tfrac{1}{12}\cos^2\theta - \tfrac{1}{12}\tilde{\xi}^2\cos^2\theta + \tfrac{1}{4}s^2 + \tfrac{1}{4}s^2\tilde{\xi}^4 - \tfrac{1}{2}s^2\tilde{\xi}^2\right) \end{array}\right](kh)^4 \quad (69)$$

Finally, according to Eq. (31) the frequency error for the bilinear element becomes:

$$\frac{\omega^h}{\omega} \approx 1 + \frac{\left(\tfrac{2}{3} - \tilde{\xi}^2\right)\cos^4\theta + (\tfrac{2}{3} - \tilde{\xi}^2)s^2\sin^4\theta}{8}(kh)^2 + O(kh)^4 \quad (70)$$

Obviously, if we take $\tilde{\xi} = \pm\sqrt{2/3}$, namely, the quadrature rule as:

$$\begin{cases} \tilde{\xi}_1 = -\sqrt{\tfrac{2}{3}},\ \tilde{\xi}_2 = \sqrt{\tfrac{2}{3}} \\ \varpi_1 = \varpi_2 = 1 \end{cases} \quad (71)$$

Equation (70) would give us a superconvergent formulation with an accuracy order of 4. Meanwhile, this superconvergent formulation completely eliminates the convergence order dependence on the wave propagation angle θ and the length/height ratio s. A superaccurate dispersion error analysis [41] also leads to the quadrature rule in Eq. (71). Nonetheless, the interesting and important fact herein is that the integration rule in Eq. (71) is the 2D tensor product form of the 1D quadature rule that exactly integrates the 1D higher order mass matrix as discussed in Eqs. (13) and (16). Meanwhile, the same quadrature rule is adopted for both mass and stiffness matrices. The present formulation distinguishes itself from the higher order mass matrix formulation where only the mass matrix is optimized. Thus we refer the present formulation as the quadrature-based superconvergent formulation (QSF). On the other hand, the present formulation does reduce to the higher order mass matrix formulation in 1D case.

5.2 Quadrature-based superconvergent formulation for 3D trilinear element

At this point, a natural question to ask is that whether a direct generalization of the quadrature rule of Eq. (71) to 3D case also provides a superconvergent formulation for the frequency computation without wave propagation direction dependence. The answer is yes and we shall prove this result in this sub-section.

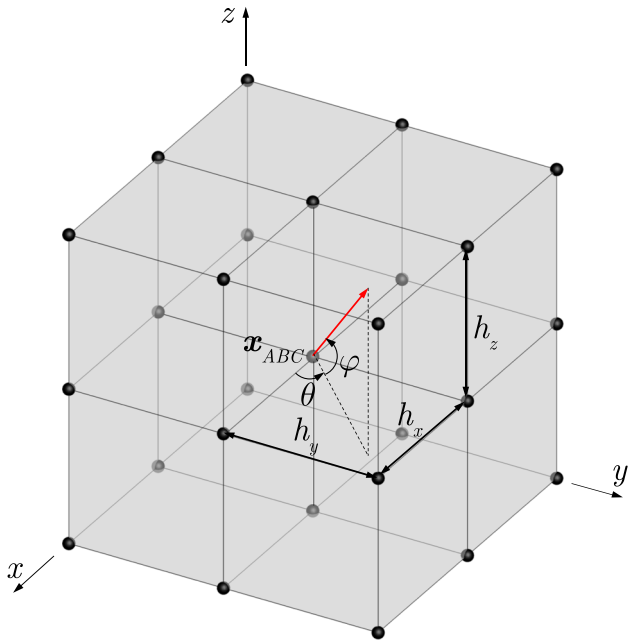

Fig. 10 A finite mesh with trilinear rectangular elements

Consider a uniform discretization with 3D trilinear rectangular elements as shown in Fig. 10, the length, width and height for a generic element are denoted by h_x, h_y and h_z, the Jacobian for a rectangular element is $J = h_x h_y h_z/8$. By employing the quadrature rule of Eq. (71) with a tensor product operation, the mass matrix for a 3D trilinear element is then computed as follows:

Table 1 Superconvergent quadrature rules for frequency computation

p	$\tilde{\xi}_i$	ϖ_i	Degree of precision
1	$-\sqrt{2/3}$	1	1
	$\sqrt{2/3}$	1	
2	$-\sqrt{13/15}$	5/13	3
	0	16/13	
	$\sqrt{13/15}$	5/13	
3	−0.964335275880	0.199826014448	5
	−0.429352058316	0.800173985552	
	0.429352058316	0.800173985552	
	0.964335275880	0.199826014448	
4	−0.978315678013	0.121787277062	7
	−0.638731398346	0.531329254103	
	0	0.693766937669	
	0.638731398346	0.531329254103	
	0.978315678013	0.121787277062	

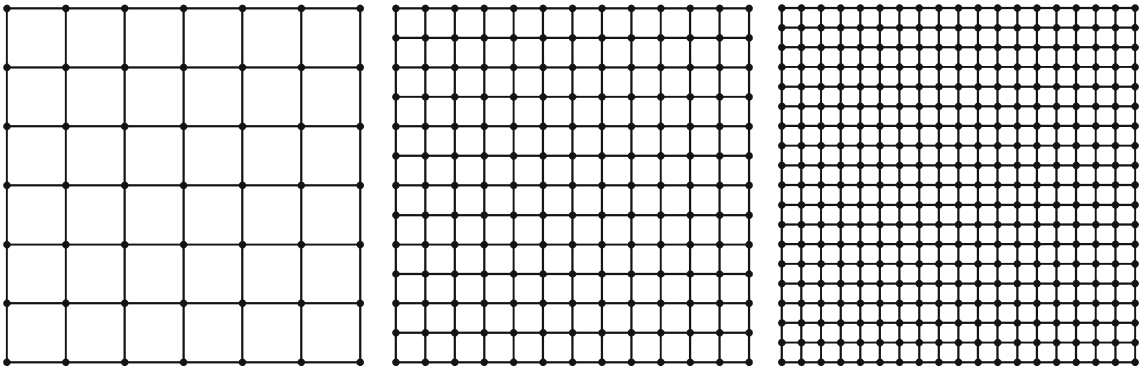

Fig. 11 Meshes for the square membrane problem using bilinear elements

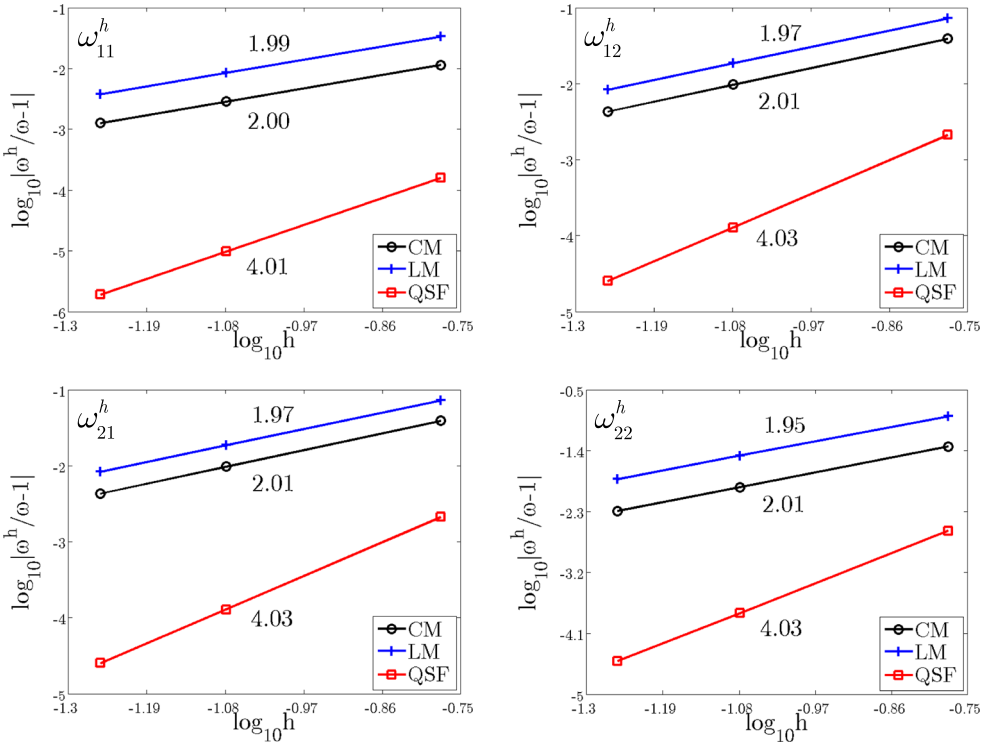

Fig. 12 Convergence comparison of the first four frequencies for the square membrane problem using bilinear elements

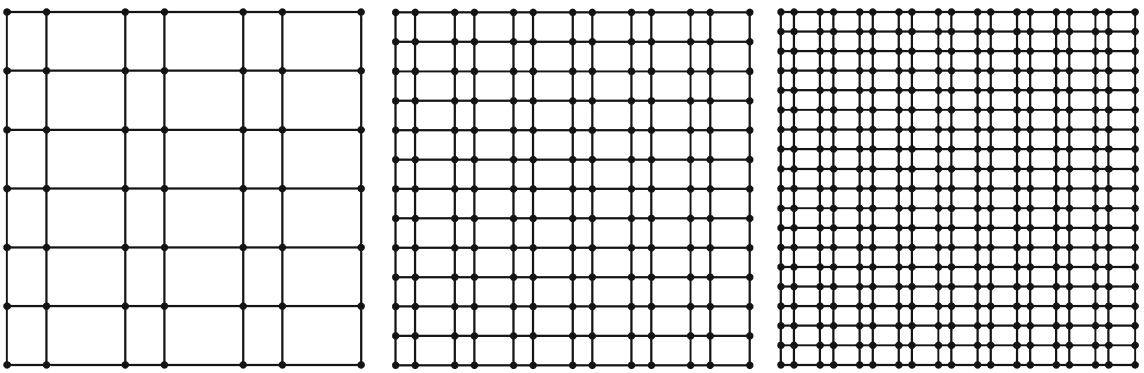

Fig. 13 Non-uniform meshes for the square membrane problem using bilinear elements

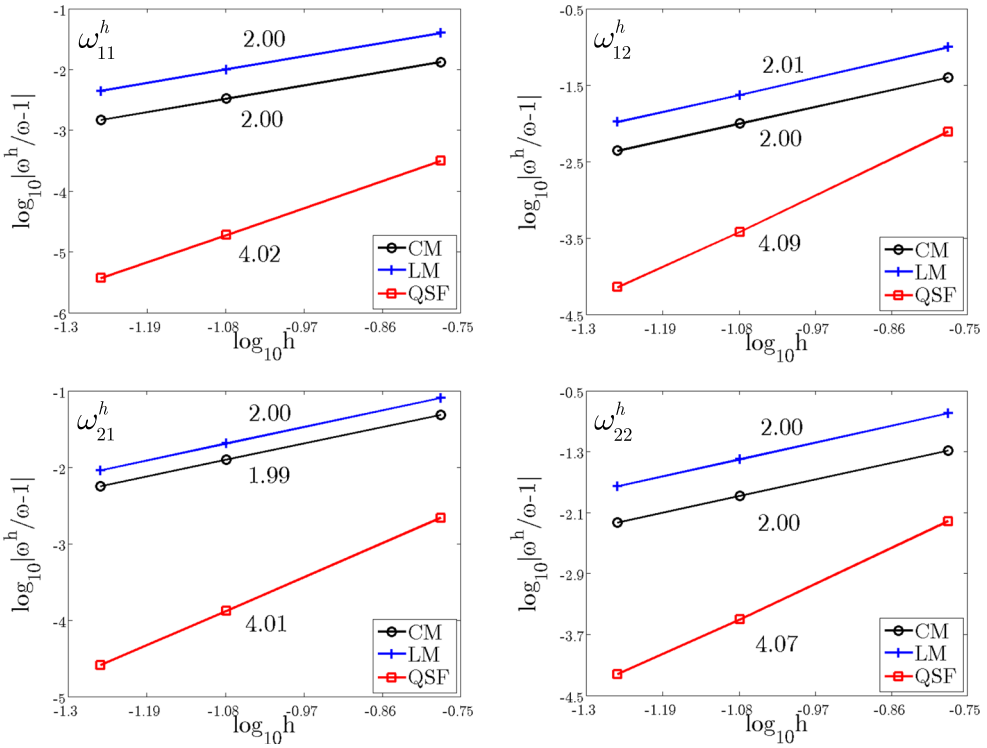

Fig. 14 Convergence comparison of the first four frequencies for the square membrane problem using bilinear elements with non-uniform meshes

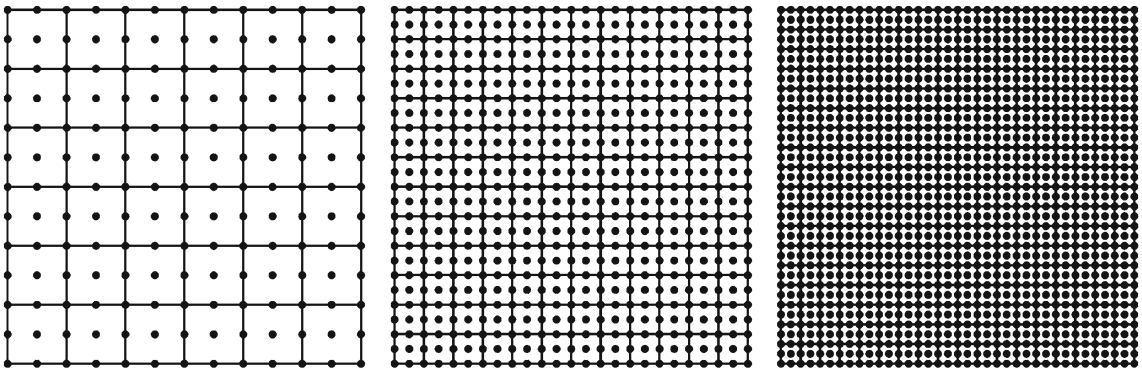

Fig. 15 Meshes for the square membrane problem using biquadratic elements

$$\tilde{\boldsymbol{M}}^e = \frac{h_x h_y h_z}{8} \sum_{i,j,k=1}^{2} \boldsymbol{N}^T(\tilde{\xi}_i, \tilde{\xi}_j, \tilde{\xi}_k)\boldsymbol{N}(\tilde{\xi}_i, \tilde{\xi}_j, \tilde{\xi}_k)\varpi_i\varpi_j\varpi_k$$
$$= \frac{h_x h_y h_z}{1728} \begin{bmatrix} 125 & 25 & 5 & 25 & 25 & 5 & 1 & 5 \\ 25 & 125 & 25 & 5 & 5 & 25 & 5 & 1 \\ 5 & 25 & 125 & 25 & 1 & 5 & 25 & 5 \\ 25 & 5 & 25 & 125 & 5 & 1 & 5 & 25 \\ 25 & 5 & 1 & 5 & 125 & 25 & 5 & 25 \\ 5 & 25 & 5 & 1 & 25 & 125 & 25 & 5 \\ 1 & 5 & 25 & 5 & 5 & 25 & 125 & 25 \\ 5 & 1 & 5 & 25 & 25 & 5 & 25 & 125 \end{bmatrix} \tag{72}$$

where the row vector $\boldsymbol{N}$ is formed by the standard eight trilinear shape functions and its gradient is denoted by $\boldsymbol{B}$ [2]. On the other hand, using the same quadrature rule defined in Eq. (71), the stiffness matrix is given by:

$$\tilde{\boldsymbol{K}}^e = \frac{c^2 h_x h_y h_z}{8} \sum_{i,j,k=1}^{2} \boldsymbol{B}^T(\tilde{\xi}_i, \tilde{\xi}_j, \tilde{\xi}_k)\boldsymbol{B}(\tilde{\xi}_i, \tilde{\xi}_j, \tilde{\xi}_k)\varpi_i\varpi_j\varpi_k$$
$$= \frac{c^2 h_x h_y h_z}{8} \begin{bmatrix} \tilde{\boldsymbol{K}}_{11}^e & \tilde{\boldsymbol{K}}_{12}^e & \tilde{\boldsymbol{K}}_{13}^e & \tilde{\boldsymbol{K}}_{14}^e \\ \tilde{\boldsymbol{K}}_{12}^{eT} & \tilde{\boldsymbol{K}}_{22}^e & \tilde{\boldsymbol{K}}_{23}^e & \tilde{\boldsymbol{K}}_{24}^e \\ \tilde{\boldsymbol{K}}_{13}^{eT} & \tilde{\boldsymbol{K}}_{23}^{eT} & \tilde{\boldsymbol{K}}_{33}^e & \tilde{\boldsymbol{K}}_{34}^e \\ \tilde{\boldsymbol{K}}_{14}^{eT} & \tilde{\boldsymbol{K}}_{24}^{eT} & \tilde{\boldsymbol{K}}_{34}^{eT} & \tilde{\boldsymbol{K}}_{44}^e \end{bmatrix} \tag{73}$$

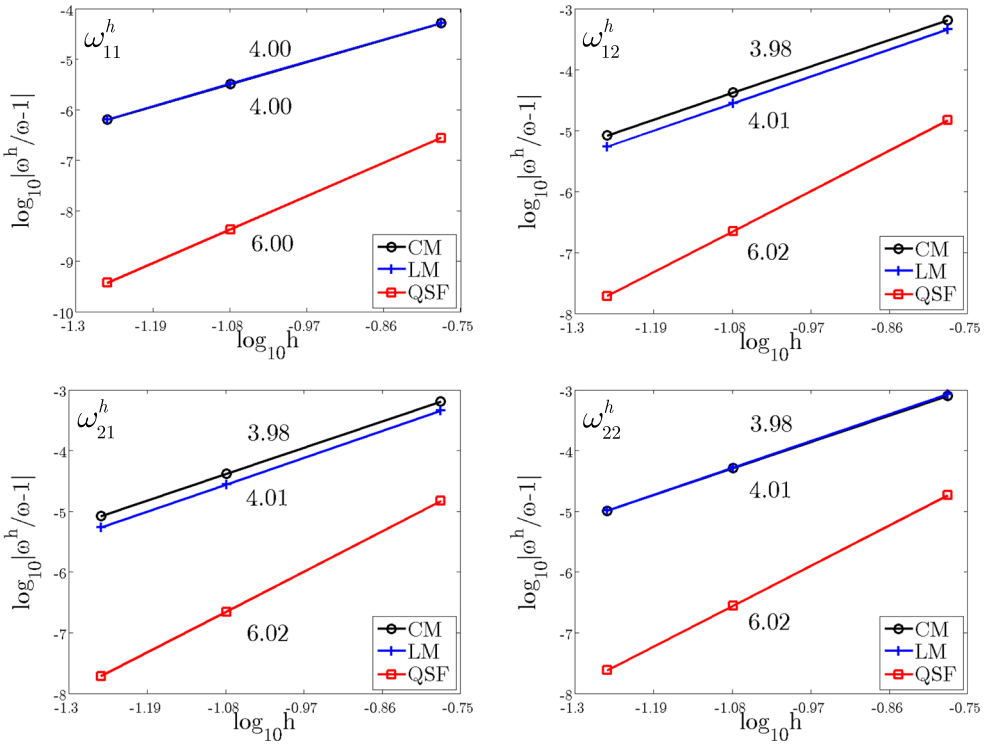

Fig. 16 Convergence comparison of the first four frequencies for the square membrane problem using biquadratic elements

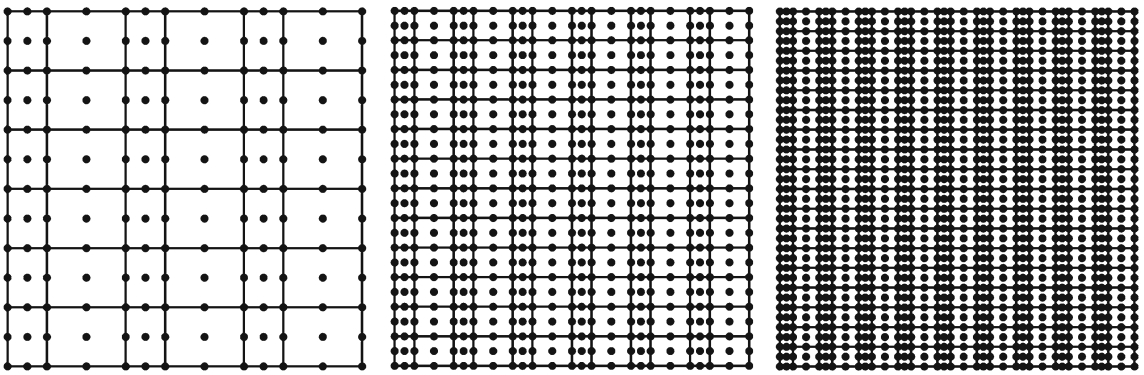

Fig. 17 Non-uniform meshes for the square membrane problem using biquadratic elements

where the sub-matrices $\tilde{\boldsymbol{K}}_{ij}^{e}{}'s$, $i, j = 1, \ldots, 4$, are given in Appendix.

Based upon Eqs. (6), (72) and (73), the stencil equation associated with the node $\boldsymbol{x}_{ABC} = (x_A, y_B, z_C)$ is:

$$\mathcal{H}(\ddot{d}_{ABC}) + c^2\mathcal{G}(d_{ABC}) = 0 \tag{74}$$

where $\mathcal{H}(\ddot{d}_{ABC})$ and $\mathcal{G}(d_{ABC})$ are given by:

$$\mathcal{H}(\ddot{d}_{ABC}) = \frac{1}{1728}$$
$$\begin{bmatrix} \ddot{d}_{(A-1)(B-1)(C+1)} + 10\ddot{d}_{(A-1)(B-1)C} + \ddot{d}_{(A-1)(B-1)(C-1)} \\ + 10\ddot{d}_{(A-1)B(C+1)} + 100\ddot{d}_{(A-1)BC} + 10\ddot{d}_{(A-1)B(C-1)} \\ + \ddot{d}_{(A-1)(B+1)(C+1)} + 10\ddot{d}_{(A-1)(B+1)C} + \ddot{d}_{(A-1)(B+1)(C-1)} \\ + 10\ddot{d}_{A(B-1)(C+1)} + 100\ddot{d}_{A(B-1)C} + 10\ddot{d}_{A(B-1)(C-1)} \\ + 100\ddot{d}_{AB(C+1)} + 1000\ddot{d}_{ABC} + 100\ddot{d}_{AB(C-1)} \\ + 10\ddot{d}_{A(B+1)(C+1)} + 100\ddot{d}_{A(B+1)C} + 10\ddot{d}_{A(B+1)(C-1)} \\ + \ddot{d}_{(A+1)(B-1)(C+1)} + 10\ddot{d}_{(A+1)(B-1)C} + \ddot{d}_{(A+1)(B-1)(C-1)} \\ + 10\ddot{d}_{(A+1)B(C+1)} + 100\ddot{d}_{(A+1)BC} + 10\ddot{d}_{(A+1)B(C-1)} \\ + \ddot{d}_{(A+1)(B+1)(C+1)} + 10\ddot{d}_{(A+1)(B+1)C} + \ddot{d}_{(A+1)(B+1)(C-1)} \end{bmatrix} \tag{75}$$

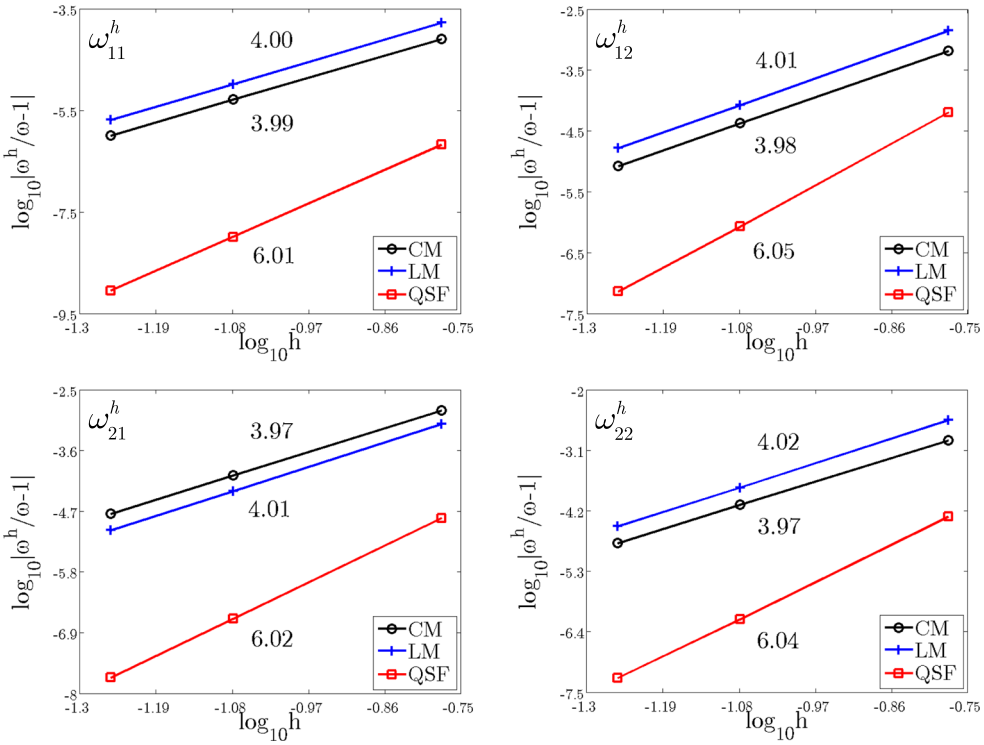

Fig. 18 Convergence comparison of the first four frequencies for the square membrane problem using biquadratic elements with non-uniform meshes

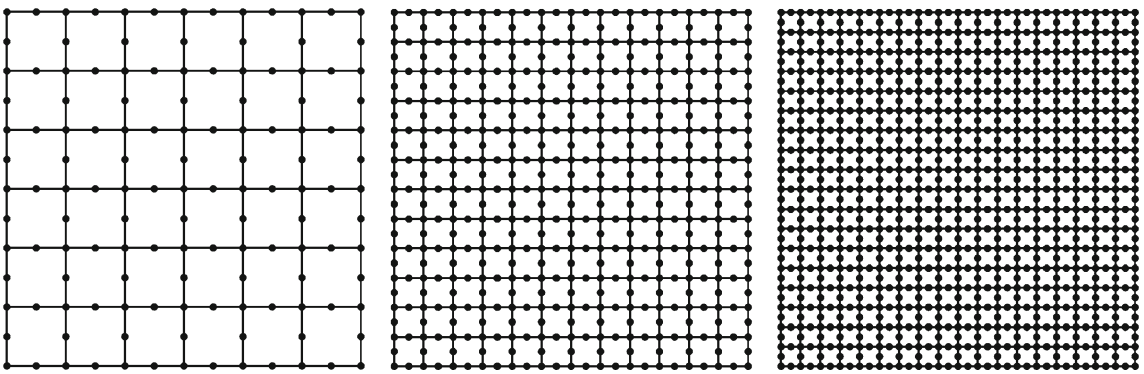

Fig. 19 Meshes for the square membrane problem using 8-node serendipity elements

$$\mathcal{G}(d_{ABC}) = \frac{1}{72}\,(D_1 + D_2 + D_3 + D_4) \tag{76}$$

where D_i 's, $i = 1, \ldots, 4$, are defined in Appendix.

Invoking the following harmonic expression for d_{ABC}:

$$\begin{cases} d_{ABC}(t) = d_0 \exp[\iota(k_x x_A + k_y y_B + k_z z_C - \omega^h t)] \\ \ddot{d}_{ABC}(t) = -(\omega^h)^2 d_0[\iota(k_x x_A + k_y y_B + k_z z_C - \omega^h t)] \end{cases} \tag{77}$$

Then Eq. (74) becomes:

$$\omega^h = c\sqrt{\frac{12\mathcal{T}}{\mathcal{S}}} \tag{78}$$

where $\mathcal{S}$ and $\mathcal{T}$ are detailed in Appendix.

Let $h_y = sh_x = sh$ and $h_z = lh_x = lh$, and introduce the following relationships:

$$k_x = k\cos\varphi\cos\theta \quad , \; k_y = k\cos\varphi\sin\theta \, , \; k_z = k\sin\varphi \tag{79}$$

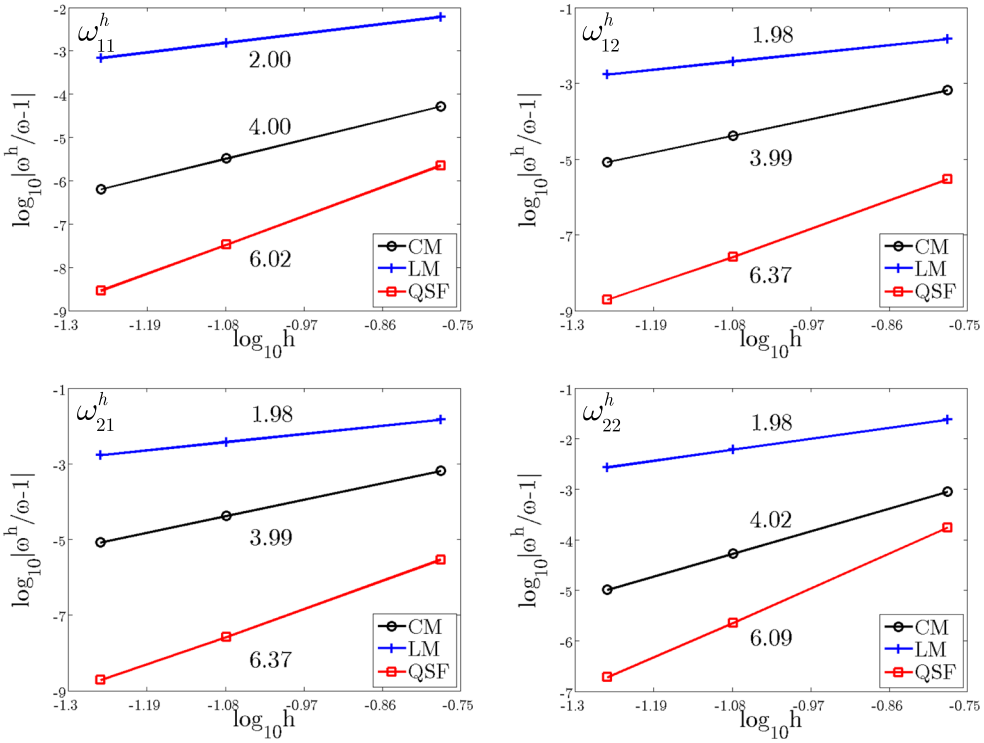

Fig. 20 Convergence comparison of the first four frequencies for the square membrane problem using 8-node serendipity elements

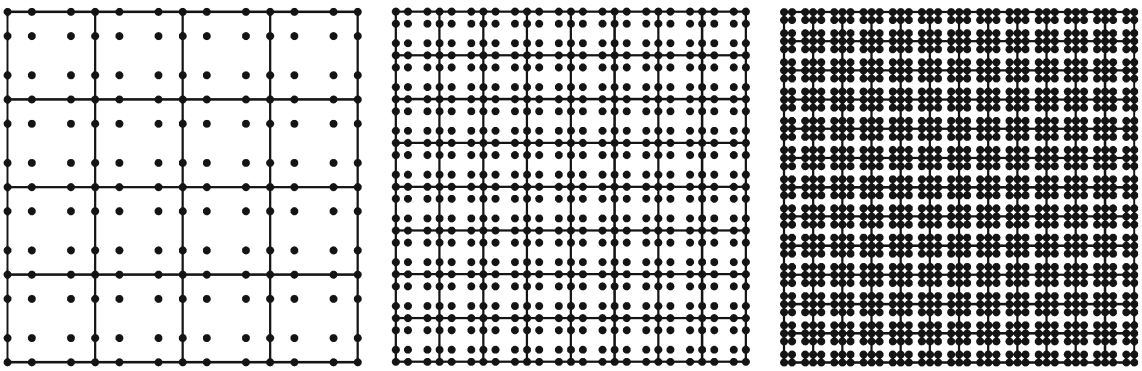

Fig. 21 Meshes for the square membrane problem using bicubic elements

in which θ and φ are the wave propagation angles as illustrated in Fig. 10. Accordingly, after proper Taylor's expansion and using $\omega = kc$, Eq. (78) reduces to:

$$\frac{\omega^h}{\omega} \approx \sqrt{\frac{864 + \chi_2 (kh)^2 + \chi_4 (kh)^4}{864 + \phi_2 (kh)^2 + \phi_4 (kh)^4}} \approx 1 + \frac{\chi_2 - \phi_2}{1728}(kh)^2 + O(kh)^4 \tag{80}$$

with

$$\begin{aligned}\chi_2 = {} & -72\cos^4\varphi\cos^4\theta + (-72 - 72s^2)\cos^4\varphi\cos^2\theta\sin^2\theta \\ & + (-72 - 72l^2)\cos^2\varphi\cos^2\theta\sin^2\varphi - 72s^2\cos^4\varphi\sin^4\theta \\ & + (-72s^2 - 72l^2)\cos^2\varphi\sin^2\theta\sin^2\varphi - 72l^2\sin^4\varphi \end{aligned} \tag{81}$$

$$\begin{aligned}\chi_4 = {} & (6s^2 + 6s^4)\cos^6\varphi\cos^2\theta\sin^4\theta \\ & + (6s^2 + 6)\cos^6\varphi\cos^4\theta\sin^2\theta + \frac{12}{5}\cos^6\varphi\cos^6\theta \end{aligned}$$

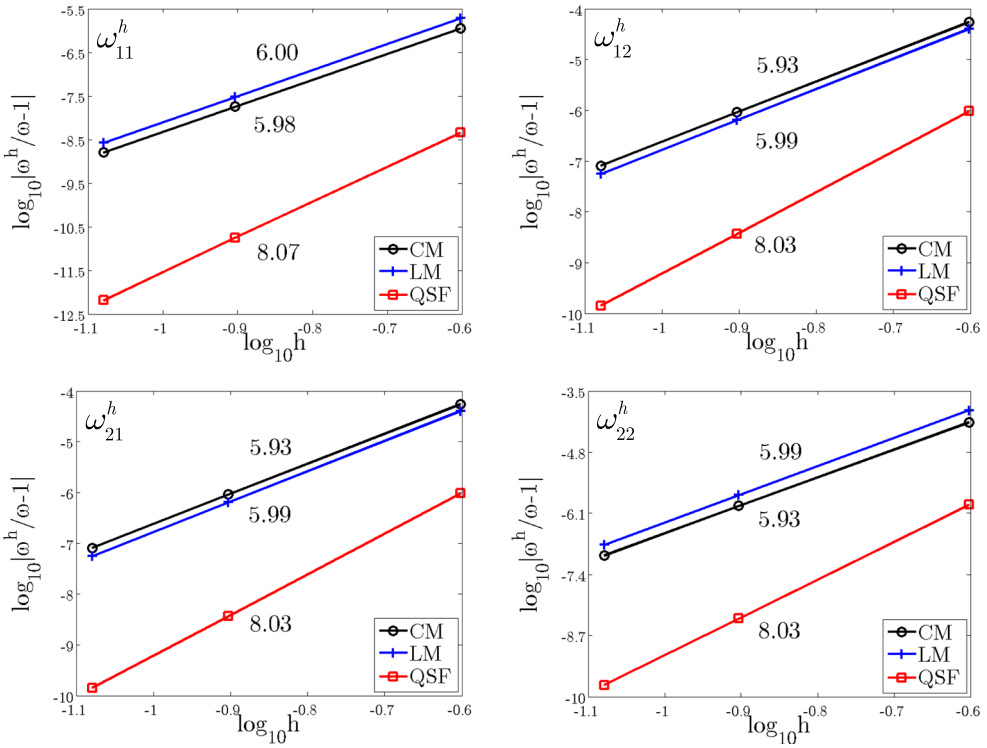

Fig. 22 Convergence comparison of the first four frequencies for the square membrane problem using bicubic elements

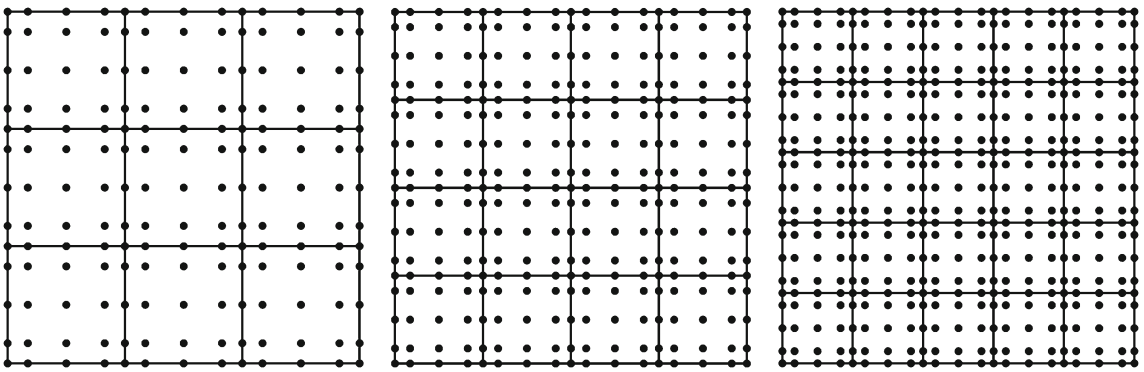

Fig. 23 Meshes for the square membrane problem using biquartic elements

$$
\begin{aligned}
&+\frac{12}{5}s^4\cos^6\varphi\sin^6\theta+(6s^2l^2+6s^4)\cos^4\varphi\sin^4\theta\sin^2\varphi\\
&+(6s^2+6l^2+6s^2l^2)\cos^4\varphi\cos^2\theta\sin^2\theta\sin^2\varphi\\
&+(6l^2+6)\cos^4\varphi\cos^4\theta\sin^2\varphi\\
&+(6l^4+6l^2s^2)\cos^2\varphi\sin^2\theta\sin^4\varphi\\
&+(6l^4+6l^2)\cos^2\varphi\cos^2\theta\sin^4\varphi+\frac{12}{5}l^4\sin^6\varphi \qquad (82)
\end{aligned}
$$

$$
\phi_2=-72s^2\cos^2\varphi\sin^2\theta-72\cos^2\varphi\cos^2\theta-72l^2\sin^2\varphi \qquad (83)
$$

$$
\begin{aligned}
\phi_4=\;&6\cos^4\varphi\cos^4\theta+6s^2l^2\cos^2\varphi\sin^2\theta\sin^2\varphi\\
&+6s^4\cos^4\varphi\sin^4\theta\\
&+6l^2\cos^2\varphi\cos^2\theta\sin^2\varphi\\
&+6s^2\cos^5\varphi\cos^3\theta\sin^2\theta+6l^4\sin^4\varphi \qquad (84)
\end{aligned}
$$

Consequently, if $\chi_2=\phi_2$ in Eq. (80), the coefficient of $(kh)^2$ vanishes and we arrive at a 4th order accurate superconvergent algorithm that does not depend on the wave propagation angles θ and φ. This identity can be easily verified as follows:

$$
\begin{aligned}
\chi_2=\;&-72\cos^4\varphi\cos^4\theta+(-72-72s^2)\cos^4\varphi\cos^2\theta\sin^2\theta\\
&+(-72-72l^2)\cos^2\varphi\cos^2\theta\sin^2\varphi-72s^2\cos^4\varphi\sin^4\theta\\
&+(-72s^2-72l^2)\cos^2\varphi\sin^2\theta\sin^2\varphi-72l^2\sin^4\varphi\\
=\;&(-72s^2\cos^2\varphi\sin^2\theta-72\cos^2\varphi\cos^2\theta-72l^2\sin^2\varphi)\\
&\times(\cos^2\varphi\cos^2\theta+\cos^2\varphi\sin^2\theta+\sin^2\varphi)\\
=\;&-72s^2\cos^2\varphi\sin^2\theta-72\cos^2\varphi\cos^2\theta-72l^2\sin^2\varphi\\
=\;&\phi_2 \qquad (85)
\end{aligned}
$$

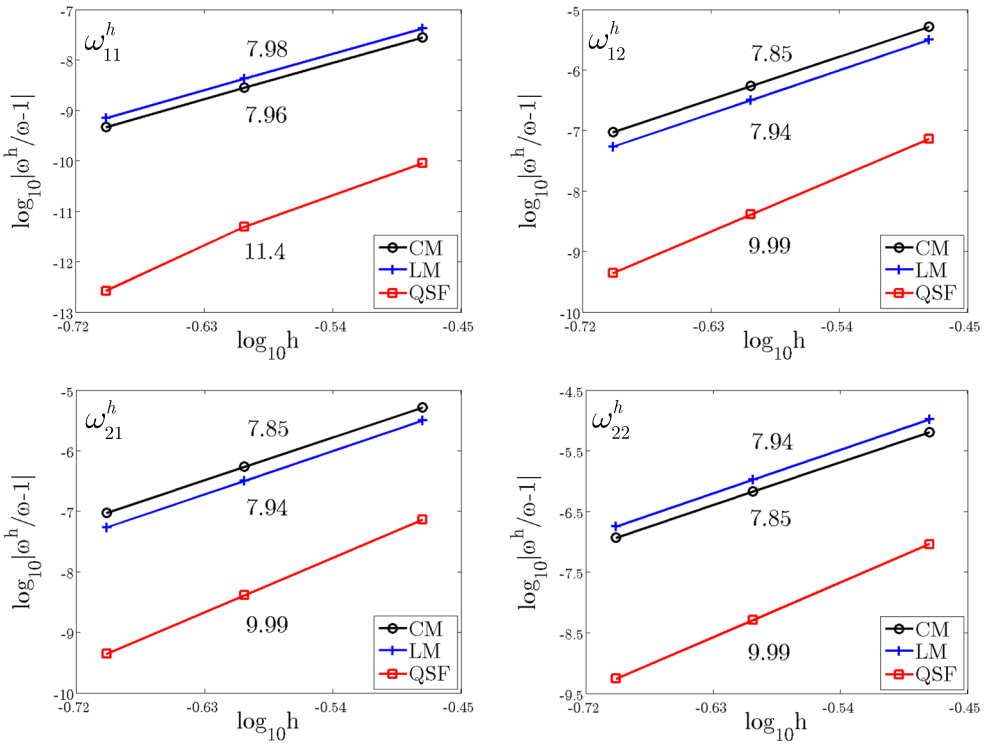

Fig. 24 Convergence comparison of the first four frequencies for the square membrane problem using biquartic elements

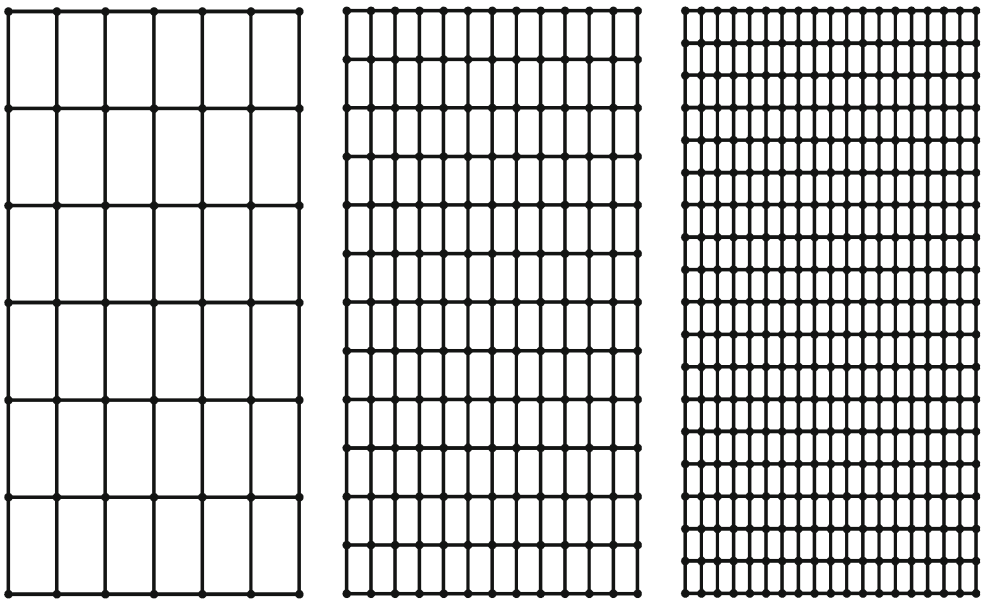

Fig. 25 Meshes for the rectangular membrane problem using bilinear elements

5.3 General quadrature-based superconvergent formulations

The quadrature rule in Eq. (71) produces the desired superconvergent formulations for 1D, 2D as well as 3D linear elements in a very simple and unified manner. One key point in this work is that the superconvergent quadrature rule can be derived from the 1D higher order mass matrix under the requirement of exact integration. Next we generalize this algorithm to higher order elements.

Consider the exact integration of the quadratic higher order mass matrix defined by Eq. (14) using three sampling

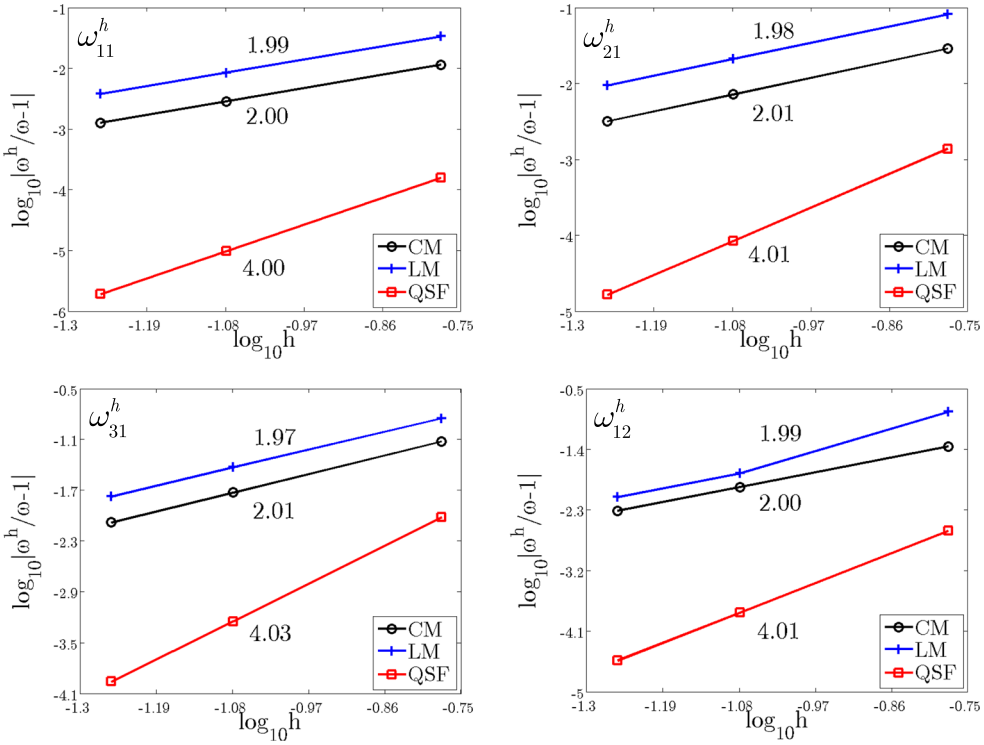

Fig. 26 Convergence comparison of the first four frequencies for the rectangular membrane problem using bilinear elements

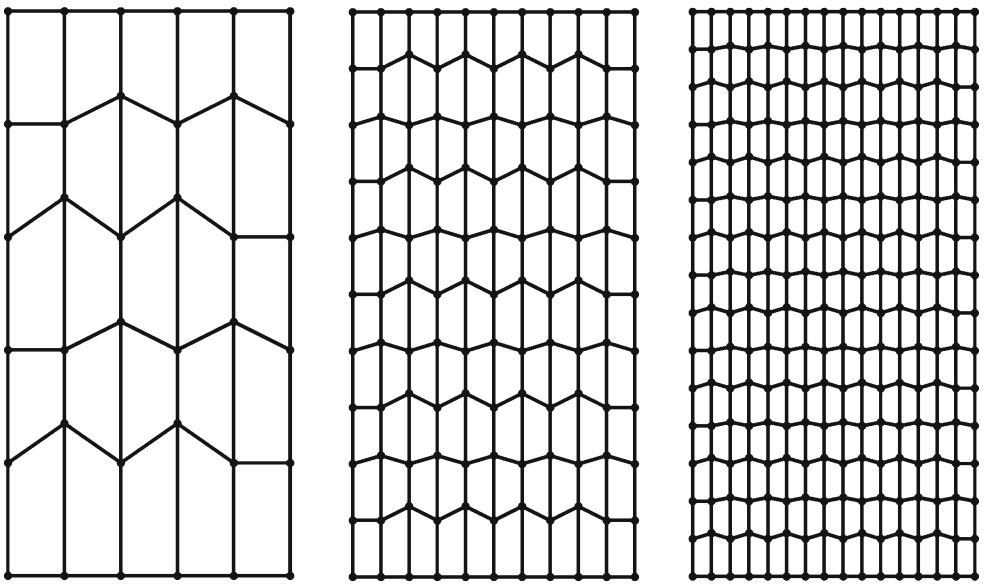

Fig. 27 Non-uniform meshes for the rectangular membrane problem using bilinear elements

points $\tilde{\xi}_1, \tilde{\xi}_2 = 0, \tilde{\xi}_3 = -\tilde{\xi}_1$, and weights $\varpi_1, \varpi_2, \varpi_3 = \varpi_1$, then the higher order mass matrix can be expressed as:

$$\boldsymbol{M}^{eh} = \sum_{i=1}^{3} \boldsymbol{N}^T(\tilde{\xi}_i)\boldsymbol{N}(\tilde{\xi}_i)J(\tilde{\xi}_i)\tilde{w}_i \tag{86}$$

where $\boldsymbol{N}(\xi) = \{N_1(\xi)\ N_2(\xi)\ N_3(\xi)\} = \{\xi(\xi-1)/2\ 1-\xi^2\ \xi(\xi+1)/2\}$, $J(\xi) = h/2$. It is straightforward to show that Eq. (86) only gives three independent equations:

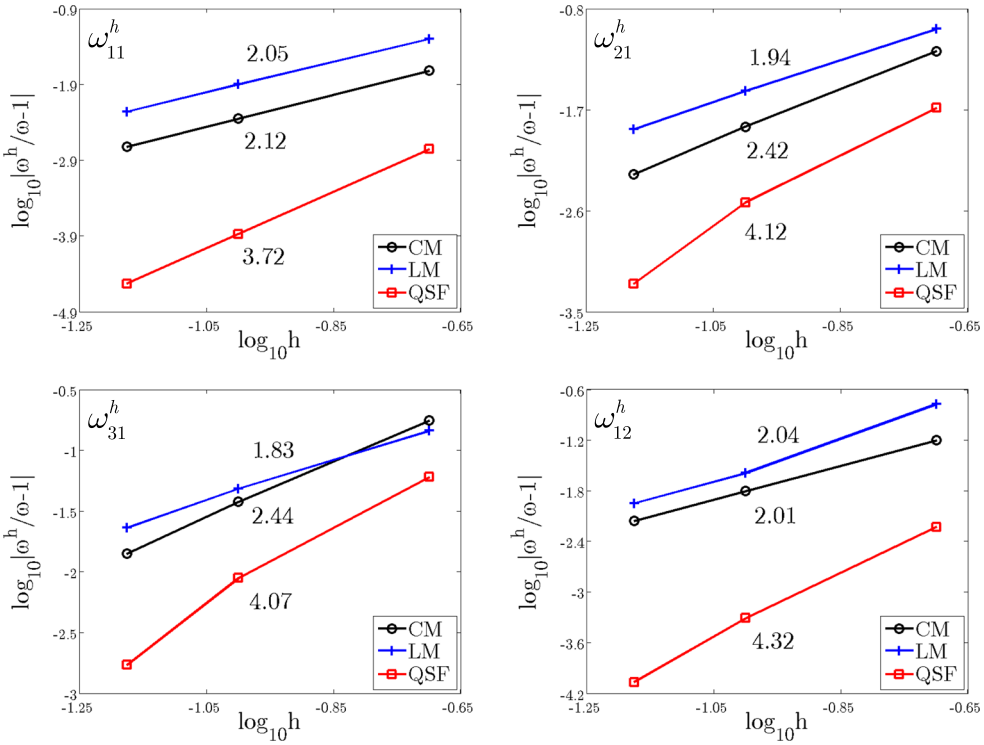

Fig. 28 Convergence comparison of the first four frequencies for the rectangular membrane problem using bilinear elements with non-uniform meshes

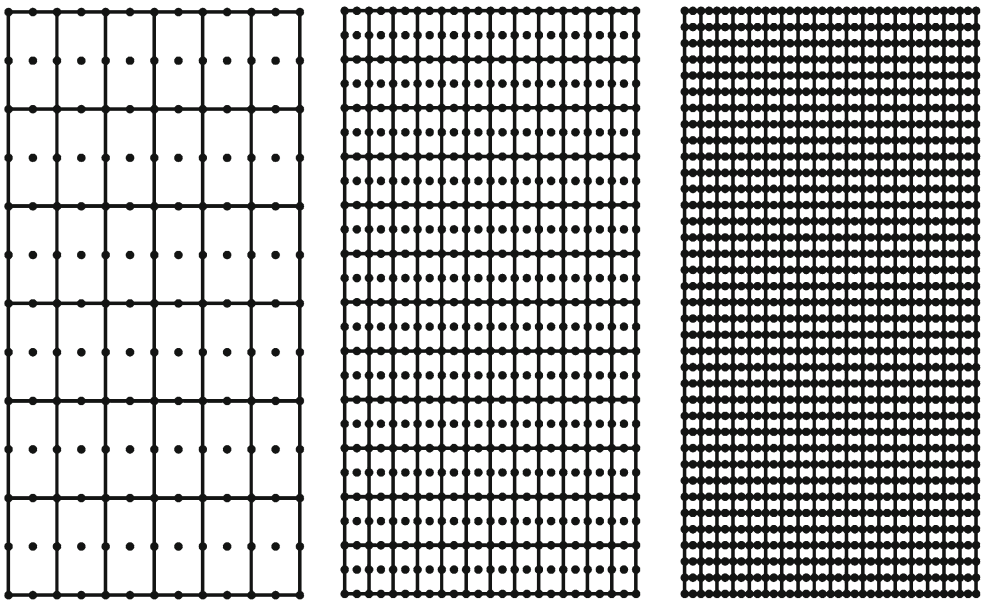

Fig. 29 Meshes for the rectangular membrane problem using biquadratic elements

$$\begin{cases} M^{eh}(1,1) = \sum_{i=1}^{3} N_1(\tilde{\xi}_i) N_1(\tilde{\xi}_i) \frac{h}{2} \varpi_i = \frac{7h}{45} \\ M^{eh}(1,3) = \sum_{i=1}^{3} N_1(\tilde{\xi}_i) N_3(\tilde{\xi}_i) \frac{h}{2} \varpi_i = -\frac{h}{90} \\ M^{eh}(2,2) = \sum_{i=1}^{3} N_2(\tilde{\xi}_i) N_2(\tilde{\xi}_i) \frac{h}{2} \varpi_i = \frac{28h}{45} \end{cases} \tag{87}$$

or

$$\begin{cases} \tilde{\xi}_1^2(\tilde{\xi}_1 - 1)^2 \varpi_1 + \tilde{\xi}_1^2(\tilde{\xi}_1 + 1)^2 \varpi_1 = \frac{56}{45} \\ \tilde{\xi}_1^2(\tilde{\xi}_1^2 - 1)\varpi_1 = -\frac{2}{45} \\ 2(1 - \tilde{\xi}_1^2)^2 \varpi_1 + \varpi_2 = \frac{56}{45} \end{cases} \tag{88}$$

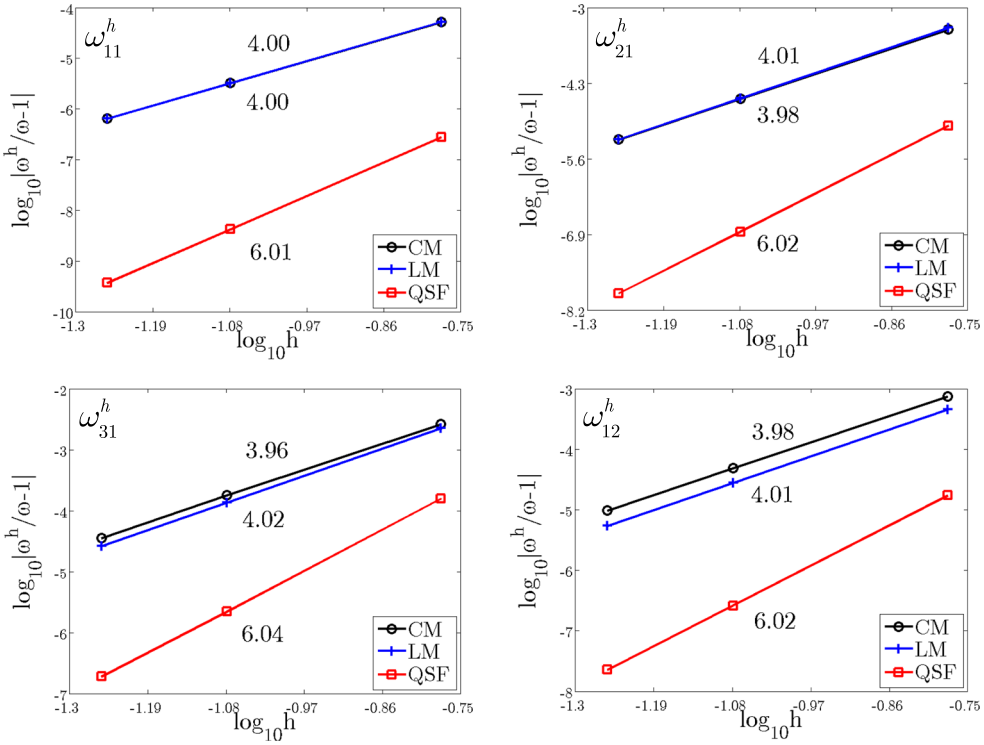

Fig. 30 Convergence comparison of the first four frequencies for the rectangular membrane problem using biquadratic elements

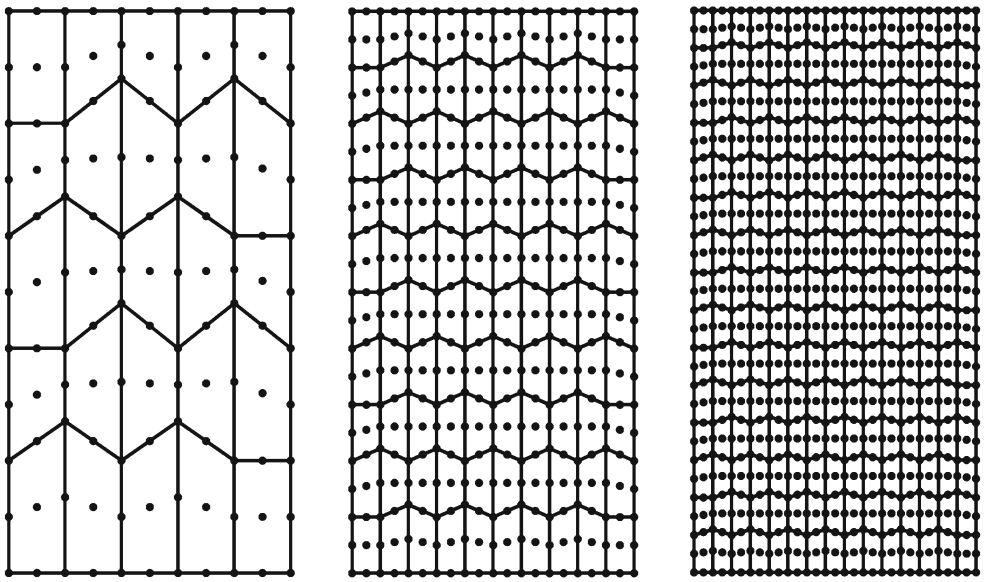

Fig. 31 Non-uniform meshes for the rectangular membrane problem using biquadratic elements

The resulting solutions for integration points and weights are:

$$\begin{cases} \tilde{\xi}_1 = -\sqrt{\frac{13}{15}}, \tilde{\xi}_2 = 0, \tilde{\xi}_3 = \sqrt{\frac{13}{15}} \\ \varpi_1 = \frac{5}{13}, \varpi_2 = \frac{16}{13}, \varpi_3 = \frac{5}{13} \end{cases} \tag{89}$$

On the other hand, an exact numerical integration for the cubic higher order mass matrix of Lobatto element in Eq. (50) requires four integration points and related weights. By symmetry, the integration points and weights can be assumed as: $\tilde{\xi}_1, \tilde{\xi}_2, \tilde{\xi}_3 = -\tilde{\xi}_2, \tilde{\xi}_4 = -\tilde{\xi}_1$, and $\varpi_1, \varpi_2, \varpi_3 = \varpi_2, \varpi_4 =$

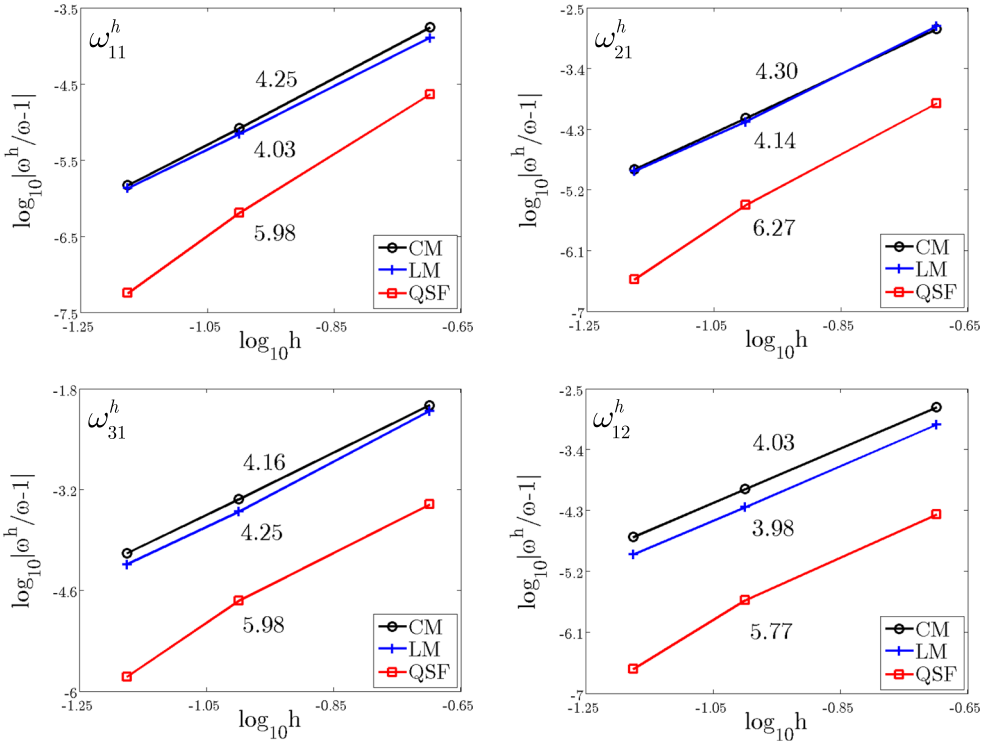

Fig. 32 Convergence comparison of the first four frequencies for the rectangular membrane problem using biquadratic elements with non-uniform meshes

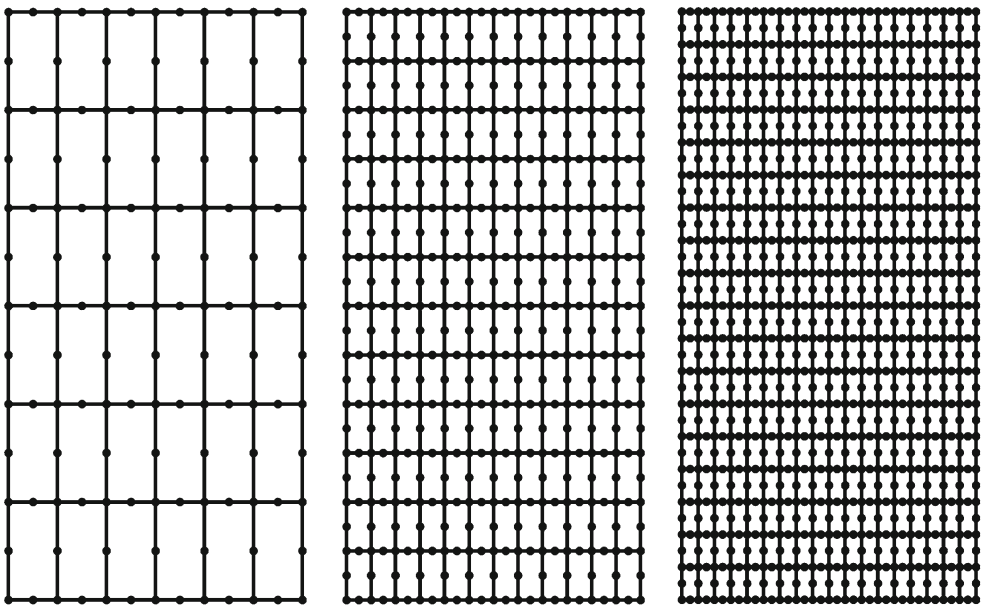

Fig. 33 Meshes for the rectangular membrane problem using 8-node serendipity elements

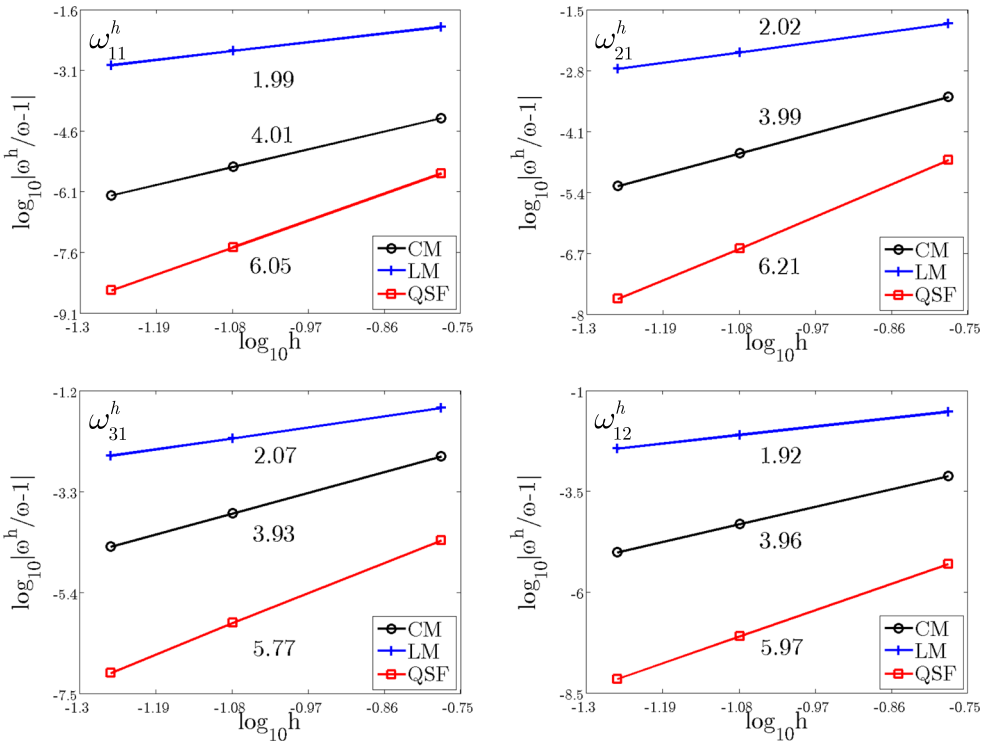

Fig. 34 Convergence comparison of the first four frequencies for the rectangular membrane problem using 8-node serendipity elements

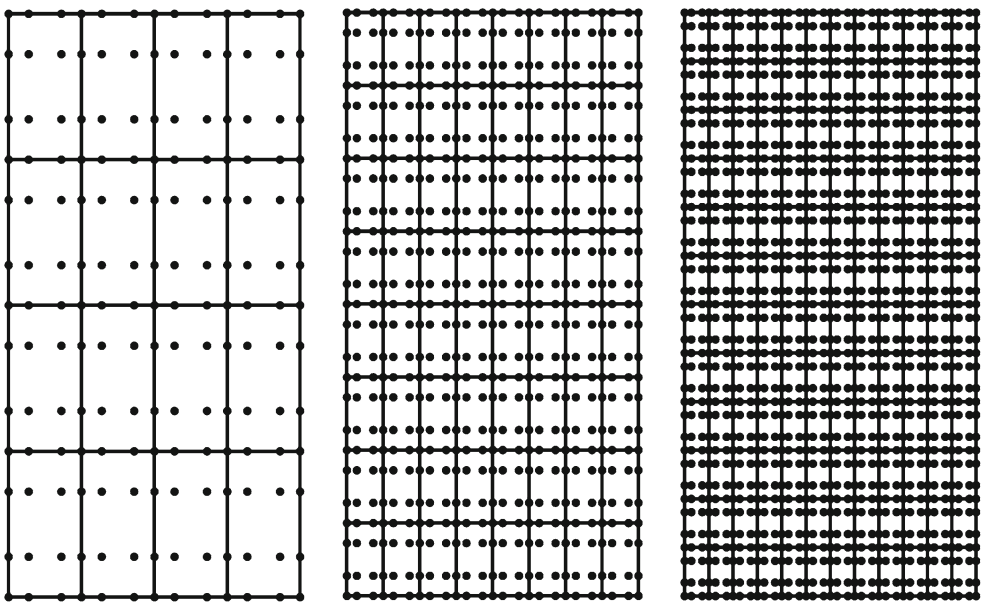

Fig. 35 Meshes for the rectangular membrane problem using bicubic elements

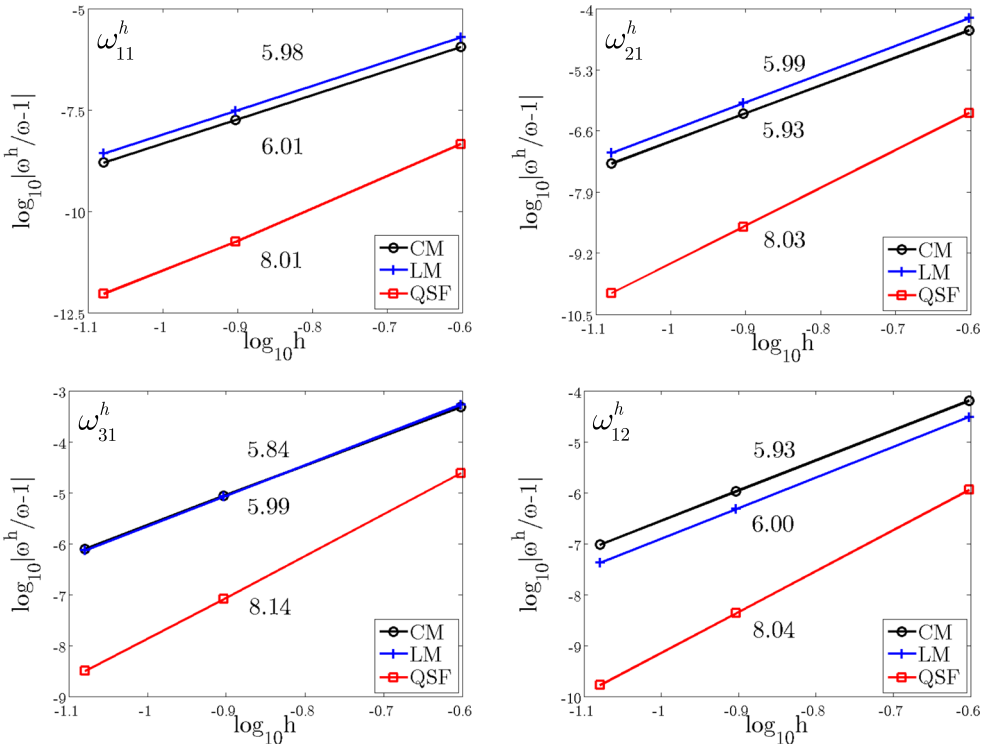

Fig. 36 Convergence comparison of the first four frequencies for the rectangular membrane problem using bicubic elements

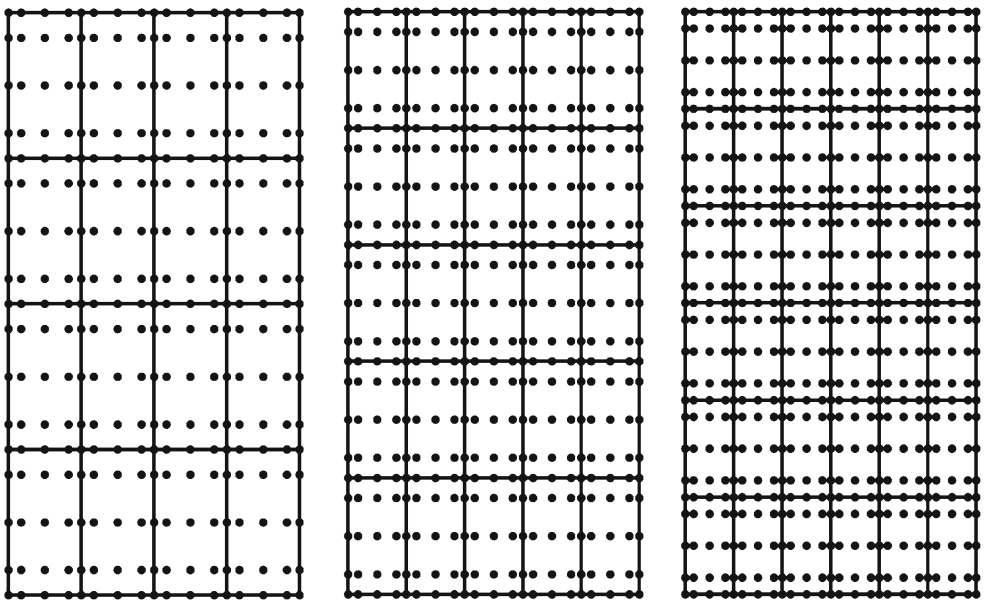

Fig. 37 Meshes for the rectangular membrane problem using biquartic elements

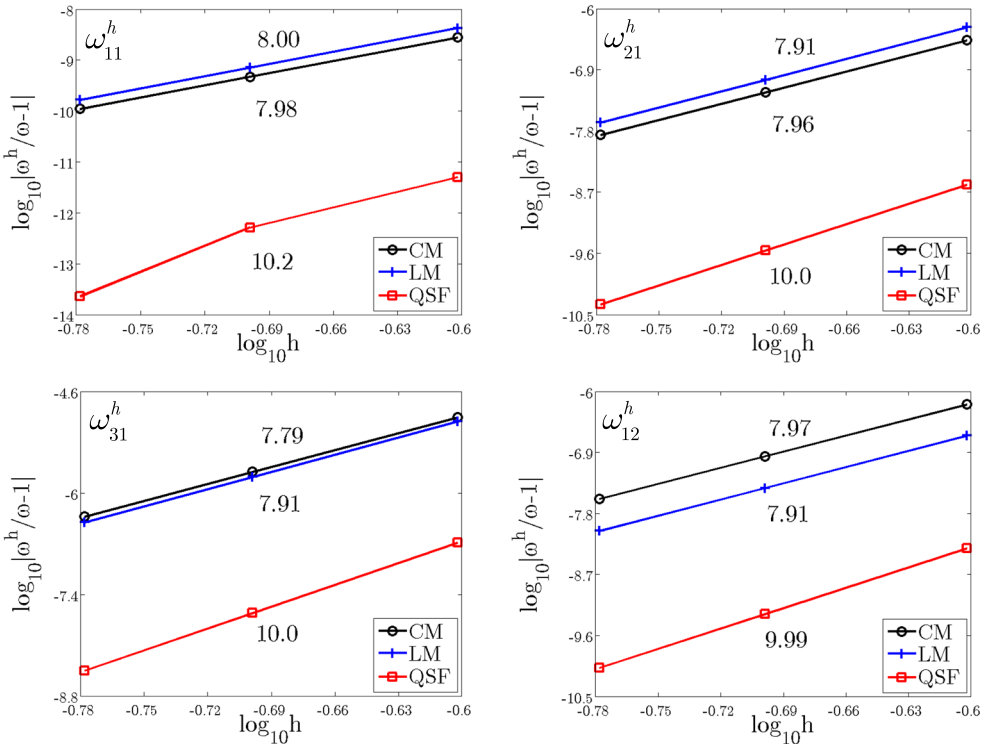

Fig. 38 Convergence comparison of the first four frequencies for the rectangular membrane problem using biquartic elements

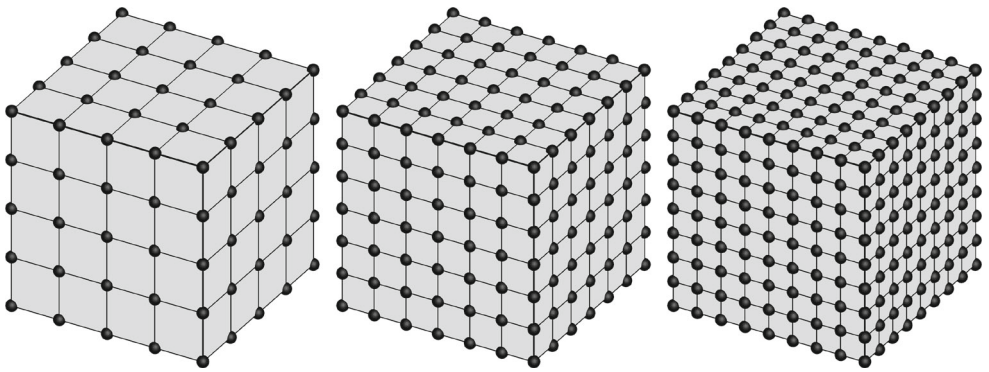

Fig. 39 3D meshes for the cubic cavity problem using trilinear elements

ϖ_1. Then the numerical integration of Eq. (50) yields four independent equations:

$$\begin{cases} M^{eh}(1,1) = \sum_{i=1}^{4} N_1(\tilde{\xi}_i) N_1(\tilde{\xi}_i) J(\tilde{\xi}_i) \tilde{w}_i = \frac{27h}{336} \\ M^{eh}(2,2) = \sum_{i=1}^{4} N_2(\tilde{\xi}_i) N_2(\tilde{\xi}_i) J(\tilde{\xi}_i) \tilde{w}_i = \frac{135h}{336} \\ M^{eh}(2,1) = \sum_{i=1}^{4} N_2(\tilde{\xi}_i) N_1(\tilde{\xi}_i) J(\tilde{\xi}_i) \tilde{w}_i = \frac{\sqrt{5}h}{336} \\ M^{eh}(1,4) = \sum_{i=1}^{4} N_1(\tilde{\xi}_i) N_4(\tilde{\xi}_i) J(\tilde{\xi}_i) \tilde{w}_i = \frac{h}{336} \end{cases} \tag{90}$$

where the shape functions $N_a's$ are given in Eq. (20). An expansion of Eq. (90) yields:

$$\begin{cases} \left(25\tilde{\xi}_1^6 + 15\tilde{\xi}_1^4 - 9\tilde{\xi}_1^2\right)\varpi_1 \\ \quad + \left(25\tilde{\xi}_2^6 + 15\tilde{\xi}_2^4 - 9\tilde{\xi}_2^2\right)\varpi_2 = \frac{29}{7} \\ \left(25\tilde{\xi}_1^6 - 45\tilde{\xi}_1^4 + 15\tilde{\xi}_1^2\right)\varpi_1 \\ \quad + \left(25\tilde{\xi}_2^6 - 45\tilde{\xi}_2^4 + 15\tilde{\xi}_2^2\right)\varpi_2 = \frac{1}{7} \\ \left(-25\tilde{\xi}_1^6 + 30\tilde{\xi}_1^4 - 5\tilde{\xi}_1^2\right)\varpi_1 \\ \quad + \left(-25\tilde{\xi}_2^6 + 30\tilde{\xi}_2^4 - 5\tilde{\xi}_2^2\right)\varpi_2 = \frac{4}{21} + \sqrt{5} \\ \left(-25\tilde{\xi}_1^6 + 35\tilde{\xi}_1^4 - 11\tilde{\xi}_1^2\right)\varpi_1 \\ \quad + \left(-25\tilde{\xi}_2^6 + 35\tilde{\xi}_2^4 - 11\tilde{\xi}_2^2\right)\varpi_2 = -\frac{17}{21} \end{cases} \tag{91}$$

From Eq. (91), the four integration points and corresponding weights for cubic Lobatto element can be solved as:

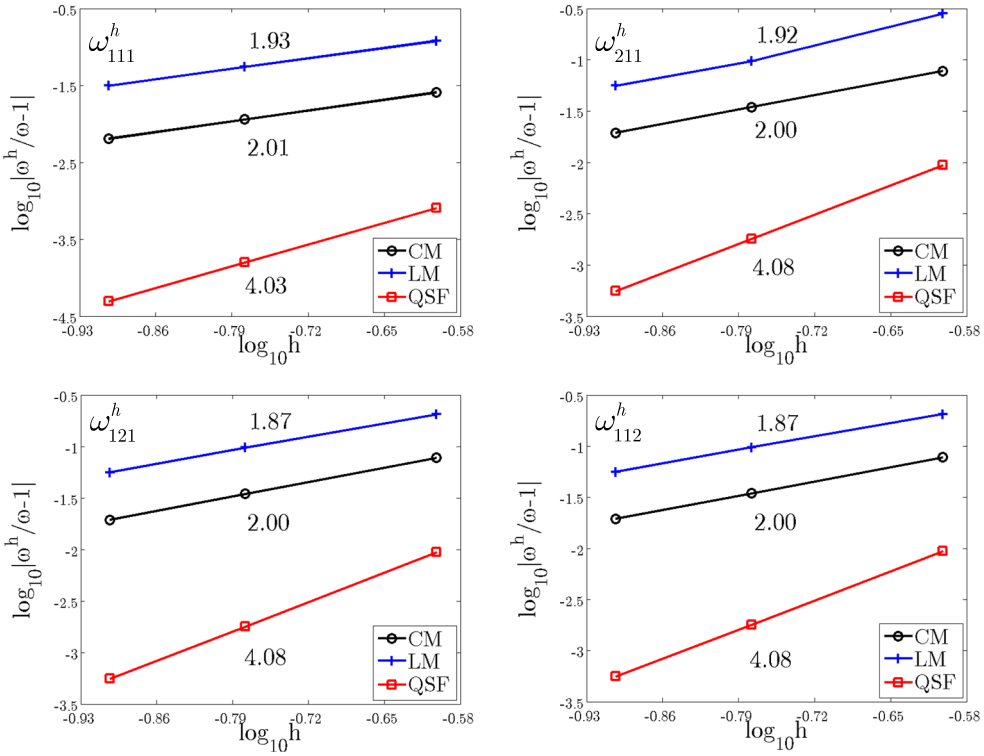

Fig. 40 Convergence comparison of the first four frequencies for the cubic cavity problem using trilinear elements

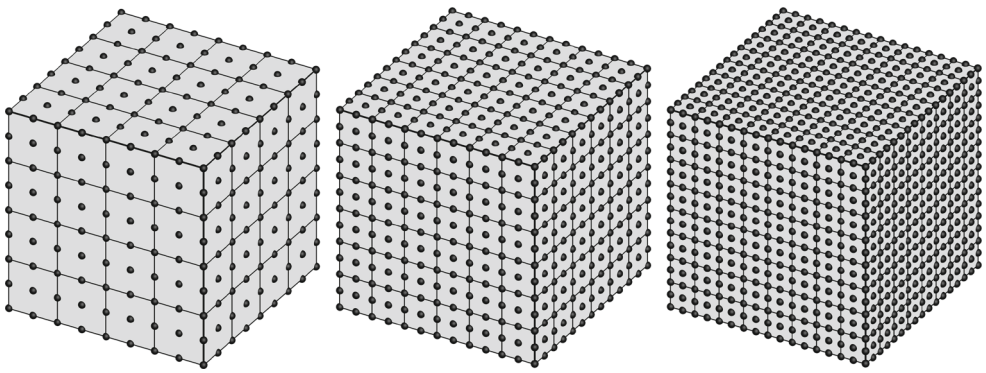

Fig. 41 3D meshes for the cubic cavity problem using triquadratic elements

$$\begin{cases} \tilde{\xi}_1 = 0.964335275880,\ \tilde{\xi}_2 = 0.429352058316, \\ \quad \tilde{\xi}_3 = -\tilde{\xi}_2,\ \tilde{\xi}_4 = -\tilde{\xi}_1 \\ \varpi_1 = 0.199826014448,\ \varpi_2 = 0.800173985552, \\ \quad \varpi_3 = \varpi_2,\ \varpi_4 = \varpi_1 \end{cases} \tag{92}$$

A similar derivation also applies to the higher order mass matrix of quartic Lobatto element. All the results of quadrature rules corresponding to linear, quadratic, cubic and quartic Lobatto elements are tabulated in Table 1, and the degree of precision for each integration rule is given as well. Consequently, a unified formulation can be established to achieve superconvergent eigenvalue computation of 1D, 2D and 3D wave equations by employing the quadrature rules in Table 1 for both the stiffness and mass matrices. For example, the 3D formulation is given as:

$$\tilde{\boldsymbol{M}}^e = \sum_{i,j,k=1}^{\tilde{n}_{\text{int}}} \boldsymbol{N}^T(\tilde{\xi}_i, \tilde{\xi}_j, \tilde{\xi}_k)\boldsymbol{N}(\tilde{\xi}_i, \tilde{\xi}_j, \tilde{\xi}_k) J(\tilde{\xi}_i, \tilde{\xi}_j, \tilde{\xi}_k)\varpi_i\varpi_j\varpi_k \tag{93}$$

$$\tilde{\boldsymbol{K}}^e = c^2 \sum_{i,j,k=1}^{\tilde{n}_{\text{int}}} \boldsymbol{B}^T(\tilde{\xi}_i, \tilde{\xi}_j, \tilde{\xi}_k)\boldsymbol{B}(\tilde{\xi}_i, \tilde{\xi}_j, \tilde{\xi}_k) J(\tilde{\xi}_i, \tilde{\xi}_j, \tilde{\xi}_k)\varpi_i\varpi_j\varpi_k \tag{94}$$

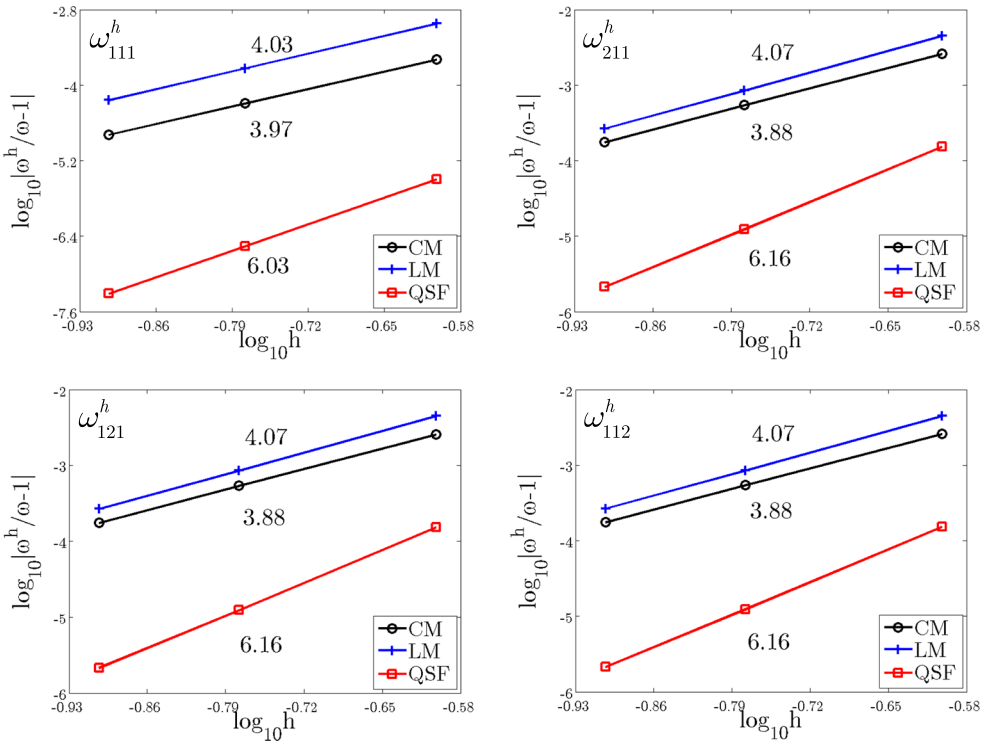

Fig. 42 Convergence comparison of the first four frequencies for the cubic cavity problem using triquadratic elements

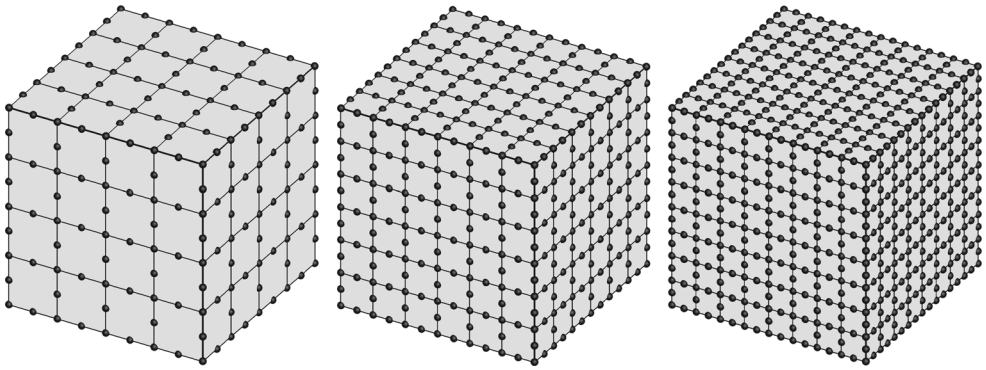

Fig. 43 3D meshes for the cubic cavity problem using 20-node serendipity elements

where $\tilde{n}_{\text{int}}$ denotes the number of integration points in each direction as shown in Table 1. It turns out that the pth order quadrature rule in Table 1 exactly integrate 1D stiffness matrix of a given pth order element as well. Therefore, the proposed quadrature-based superconvergent formulation reduces to the higher order mass matrix formulation in 1D case. While in multidimensional cases, the present method is not equivalent to the higher order mass matrix formulation and the wave propagation angle dependence arising from the frequency computation is completely removed by the proposed algorithm with trivial numerical implementation.

6 Numerical demonstration

6.1 2D square membrane problem

Consider the free vibration of a square membrane that is subjected to a fixed boundary condition, the analytical solution of the vibration frequency for this problem is [43]:

$$\omega_{ij} = \frac{\pi c}{L}\sqrt{i^2 + j^2} \tag{95}$$

where L is the length of the membrane.

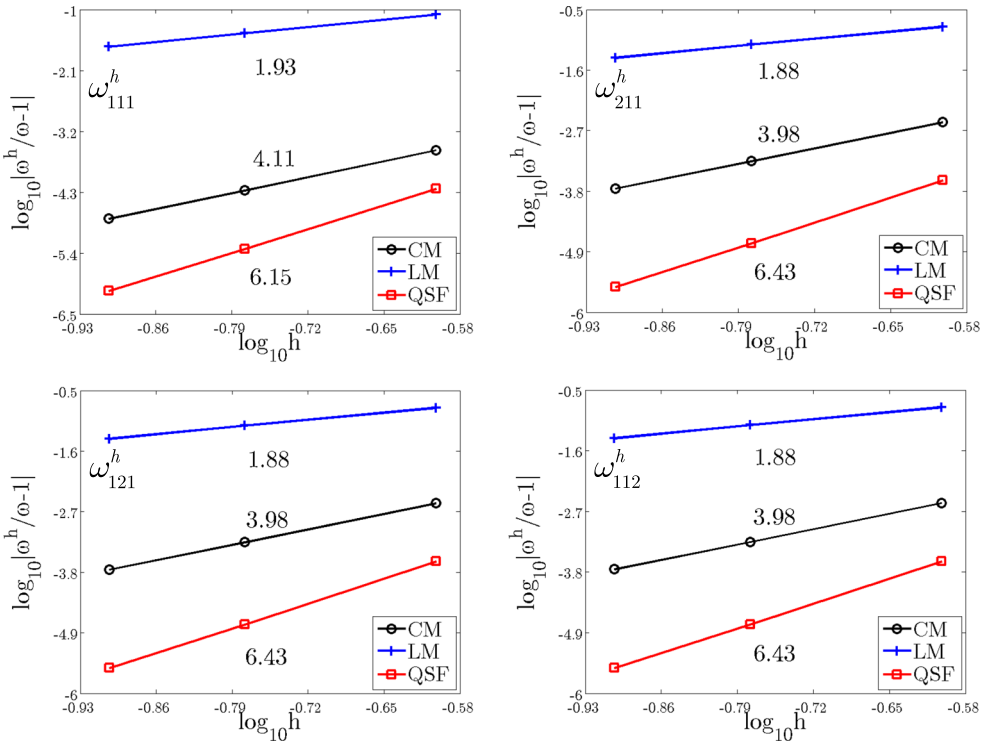

Fig. 44 Convergence comparison of the first four frequencies for the cubic cavity problem using 20-node serendipity elements

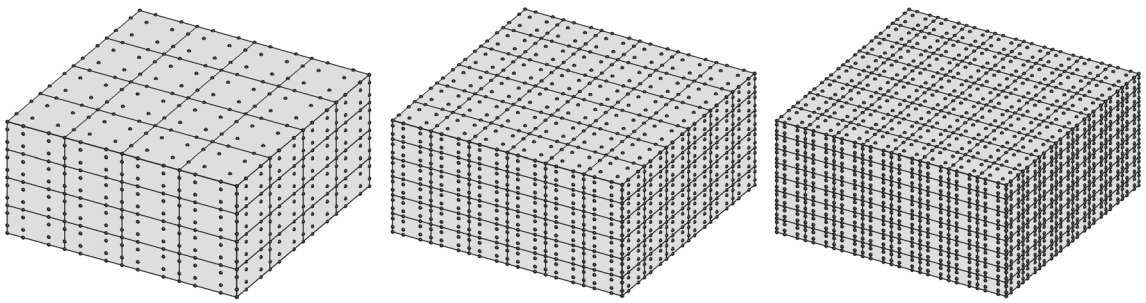

Fig. 45 3D meshes for the rectangular cavity problem using tricubic elements

In the computation, without loss of generality, we take $L = 1$ and $c = 1$. For this square membrane problem, we perform convergence tests for all four types of elements discussed previously, i.e., bilinear, biquadratic, bicubic and biquartic Lobatto elements, plus the commonly used 8-node serendipity element. Under each circumstance, the finite element meshes and corresponding convergence results for the first four frequencies are presented in a sequence. Figures 11, 12, 13, 14, 15, 16, 17, 18, 19, 20, 21, 22, 23 and 24 list the finite element meshes and frequency convergence results for this square membrane problem, where CM and LM represent the conventional consistent and lumped mass matrices by standard Gauss integration, QSF represents the proposed quadrature-based superconvergent formulation. It is evident that all the results predict a superconvergence for the proposed QSF with convergence rates of 4, 6, 8 and 10 for the bilinear, biquadratic, bicubic and biquartic Lobatto elements, while they are 2, 4, 6 and 8 for CM and LM, respectively. In particular, the non-uniform meshes as shown in Figs. 13 and 17 also produce superconvergent results of Figs. 14 and 18. Another very interesting observation is that when we directly adopt the proposed three-point quadrature rule for the 8-node serendipity element, as shown in Figs. 19 and 20, the superconvergence also occurs for the frequencies, although the superconvergent quadrature rules is designed for Lagrangian type of Lobatto elements. However, the LM of 8-node serendipity element by row sum only leads to 2nd order accurate frequencies, in contrast to the 4th order accuracy for CM and the 6th order accuracy for QSF.

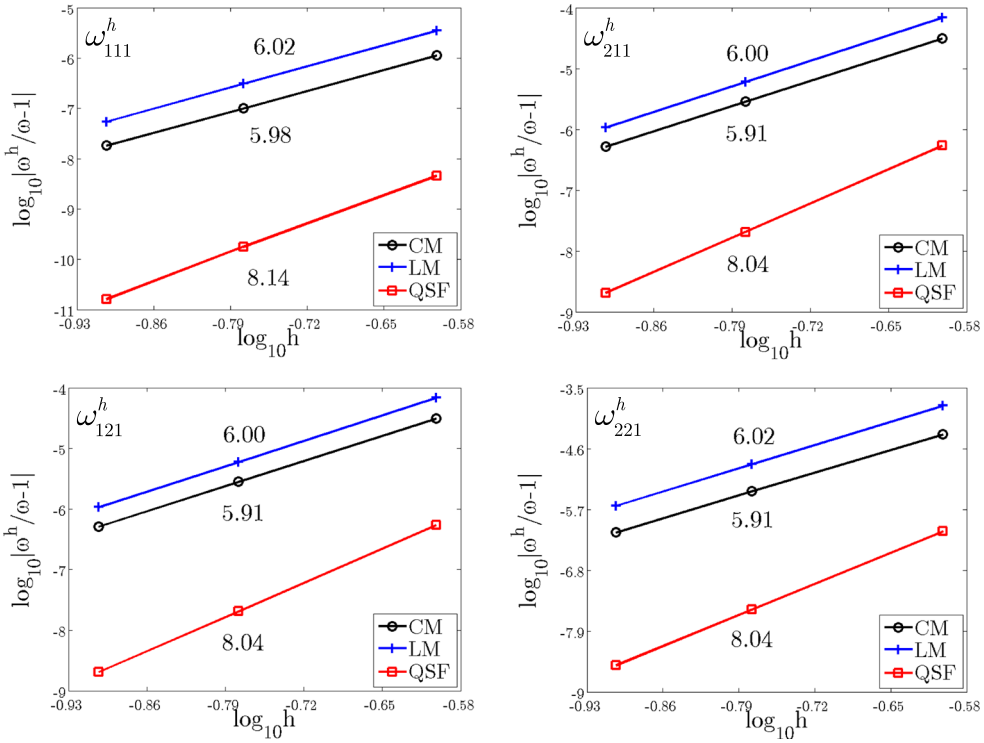

Fig. 46 Convergence comparison of the first four frequencies for the rectangular cavity problem using tricubic elements

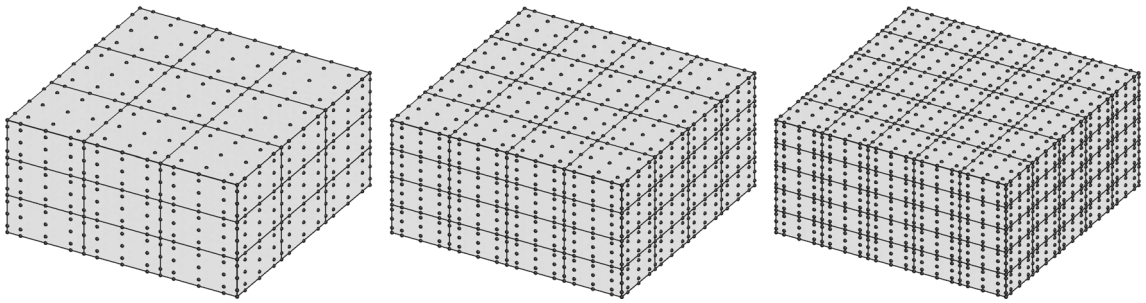

Fig. 47 3D meshes for the rectangular cavity problem using triquartic elements

6.2 2D rectangular membrane problem

It is noted that the HOM in Eq. (15) is only applicable to square elements. In order to comprehensively assess the proposed method, the rectangular membrane with four fixed sides is further studied herein. This rectangular membrane has length L_x and width L_y and its analytical frequency ω_{ij} can be expressed as [43]:

$$\omega_{ij} = \pi c \sqrt{\left(\frac{i}{L_x}\right)^2 + \left(\frac{j}{L_y}\right)^2} \tag{96}$$

In the finite element analysis, we assume $c = 1$, $L_x = 1$ and $L_y = 2$. Similar to the square membrane problem, the finite element discretizations and results of frequency convergence are sequentially presented in Figs. 25, 26, 27, 28, 29, 30, 31, 32, 33, 34, 35, 36, 37 and 38, for the bilinear, biquadratic, serendipity, bicubic and biquartic elements. The results consist of the first four frequencies using three formulations, namely, CM, LM and QSF, as again reveal that the proposed QSF gives a very superior performance compared with CM and LM. The superconvergence is consistently observed, which is proved by the frequency convergence rates of 4, 6, 8 and 10 for the bilinear, biquadratic, bicubic and biquartic Lobatto elements, i.e. two additional orders of accuracy are gained by the proposed QSF in comparison with CM and LM. At the same time, even when the non-uniform meshes of Figs. 27 and 31 are used for this rectangular membrane, as can be seen from Figs. 28 and 32, the present QSF also preforms very well in contrast to CM and LM. Moreover, although the proposed three-point quadrature rule is designed for the biquadratic element, a direct adoption of this integration rule

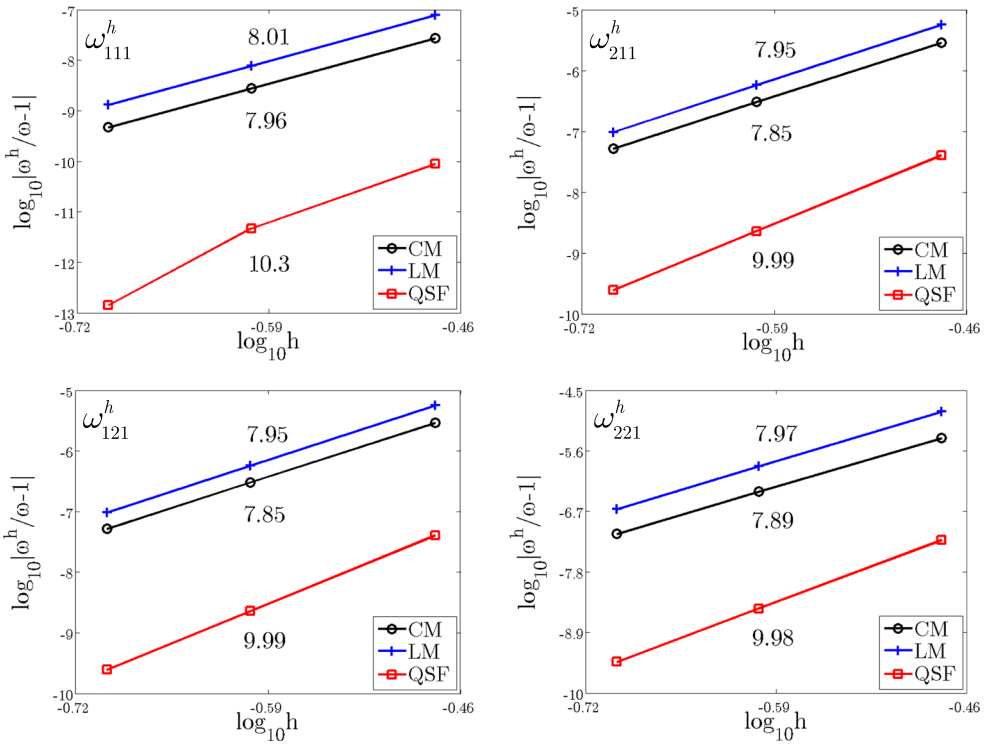

Fig. 48 Convergence comparison of the first four frequencies for the rectangular cavity problem using triquartic elements

for the 8-node serendipity element yields superconvergent results with 6th order accuracy as well, which is clearly demonstrated in Figs. 33 and 34, but LM in this case only gives 2nd order accurate frequencies, two orders lower than CM.

6.3 3D cubic and rectangular cavity problems

One strength of the proposed method is its easiness of extension to 3D problems. Here we investigate its performance for 3D problems. Two typical examples are considered, i.e., the cubic and rectangular cavity problems and the frequencies of acoustic pressure in these domains are searched. The length, width and height of rectangular cavity are denoted by L_x, L_y and L_z, if a homogenous boundary condition is assumed, the analytical frequency solution for this problem is [43]:

$$\omega_{ijk} = \pi c \sqrt{\left(\frac{i}{L_x}\right)^2 + \left(\frac{j}{L_y}\right)^2 + \left(\frac{k}{L_z}\right)^2} \tag{97}$$

This solution applies to the cubic cavity problem when $L_x = L_y = L_z$.

For brevity purpose, the trilinear, triquadratic and 20-node serendipity elements are used to compute the frequencies for the cubic cavity problem, while tricubic and triquartic elements are adopted for the frequency analysis of the rectangular cavity problem. The parameters used for the cubic and rectangular cavity problems are: $L_x = L_y = L_z = 1$ and $c = 1$; $L_x = L_y = 2$, $L_z = 1$ and $c = 1$. Figures 39, 40, 41 and 42 show the finite element meshes and frequency convergence results of the first four frequencies for the cubic cavity problem, which demonstrate that the frequency convergence rates are 2 and 4 for both CM and LM using the trilinear and triquadratic elements, but they are upgraded to 4 and 6 by the proposed QSF, i.e., superconvergence is achieved for this 3D problem. In case that the 20-node serendipity elements are used, as shown in Figs. 43 and 44, LM and CM produce 2nd and 4th order accurate frequencies, while once again QSF provides 6th order accurate results. The finite element discretizations and results of frequency convergence for the rectangular cavity problem are plotted in Figs. 45, 46, 47 and 48, where the tricubic and triquartic Lobatto elements are utilized. These frequency convergence results exhibit superconvergent behaviors one more time for the proposed QSF that leads to 8th and 10th order accurate frequencies, where 6th and 8th order accurate frequencies are obtained by CM and LM.

7 Conclusions

A unified quadrature-based superconvergent finite element formulation was presented to compute the eigenvalues of wave equations. The proposed formulation is built upon the

Lagrangian type of Lobatto elements with Lobatto points as the finite element nodes. In 1D setting, a general method of α mass matrix formulation was proposed to develop the higher order mass matrices for arbitrary order elements. Both theoretical proofs for linear and quadratic elements and numerical examinations for cubic and quartic elements universally demonstrated that a choice of $\alpha_{opt} = p + 1$ leads to the desired higher order mass matrices with eigenvalue or frequency superconvergence. For example, 4th, 6th, 8th and 10th order of accuracy are achieved by the higher order mass matrices, in contrast to 2nd, 4th, 6th and 8th order of accuracy by the corresponding consistent and lumped mass matrices, for linear, quadratic, cubic and quartic elements, respectively. Subsequently, the multidimensional superconvergent formulation was realized through adopting a set of superconvergent quadrature rules simultaneously for the mass and stiffness matrices. Through theoretical derivations for bilinear and trilinear elements and numerical justifications for other elements, it was shown that these superconvergent quadrature rules essentially are the ones that exactly integrate the proposed 1D higher order mass matrices. The superconvergent quadrature rules for linear, quadratic, cubic and quartic elements were presented in detail. As a result, a quadrature-based superconvergent formulation was established in a unified fashion for multidimensional problems with no difficulty and complexity regarding to the numerical implementation. The proposed approach reduces to the higher order mass formulation for 1D problems since these superconvergent quadrature rules exactly integrate 1D higher order mass and stiffness matrices. At the same time, without the requirement of further effort, the present quadrature-based superconvergent formulation completely eliminates the wave propagation direction dependence issue associated with the multidimensional higher order mass matrix formulation. The expected superconvergence in the frequency computation of wave equations is well demonstrated by numerical examples.

Acknowledgements The support of this work by the National Natural Science Foundation of China (11472233, 11222221) and the Natural Science Foundation of Fujian Province of China (2014J06001) is gratefully acknowledged.

Appendix

The sub-matrices $\tilde{\boldsymbol{K}}^e_{ij}$'s in Eq. (73) are defined as follows:

$$\tilde{\boldsymbol{K}}^e_{11} = \begin{bmatrix} \frac{25}{18h_x^2}+\frac{25}{18h_y^2}+\frac{25}{18h_z^2} & -\frac{25}{18h_x^2}+\frac{5}{18h_y^2}+\frac{5}{18h_z^2} \\ -\frac{25}{18h_x^2}+\frac{5}{18h_y^2}+\frac{5}{18h_z^2} & \frac{25}{18h_x^2}+\frac{25}{18h_y^2}+\frac{25}{18h_z^2} \end{bmatrix} \tag{98}$$

$$\tilde{\boldsymbol{K}}^e_{12} = \begin{bmatrix} -\frac{5}{18h_x^2}-\frac{5}{18h_y^2}+\frac{1}{18h_z^2} & \frac{5}{18h_x^2}-\frac{25}{18h_y^2}+\frac{5}{18h_z^2} \\ \frac{5}{18h_x^2}-\frac{25}{18h_y^2}+\frac{5}{18h_z^2} & -\frac{5}{18h_x^2}-\frac{5}{18h_y^2}+\frac{1}{18h_z^2} \end{bmatrix} \tag{99}$$

$$\tilde{\boldsymbol{K}}^e_{13} = \begin{bmatrix} \frac{5}{18h_x^2}+\frac{5}{18h_y^2}-\frac{25}{18h_z^2} & -\frac{5}{18h_x^2}+\frac{1}{18h_y^2}-\frac{5}{18h_z^2} \\ -\frac{5}{18h_x^2}+\frac{1}{18h_y^2}-\frac{5}{18h_z^2} & \frac{5}{18h_x^2}+\frac{5}{18h_y^2}-\frac{25}{18h_z^2} \end{bmatrix} \tag{100}$$

$$\tilde{\boldsymbol{K}}^e_{14} = \begin{bmatrix} -\frac{1}{18h_x^2}-\frac{1}{18h_y^2}-\frac{1}{18h_z^2} & \frac{1}{18h_x^2}-\frac{5}{18h_y^2}-\frac{5}{18h_z^2} \\ \frac{1}{18h_x^2}-\frac{5}{18h_y^2}-\frac{5}{18h_z^2} & -\frac{1}{18h_x^2}-\frac{1}{18h_y^2}-\frac{1}{18h_z^2} \end{bmatrix} \tag{101}$$

$$\tilde{\boldsymbol{K}}^e_{22} = \begin{bmatrix} \frac{25}{18h_x^2}+\frac{25}{18h_y^2}+\frac{25}{18h_z^2} & -\frac{25}{18h_x^2}+\frac{5}{18h_y^2}+\frac{5}{18h_z^2} \\ -\frac{25}{18h_x^2}+\frac{5}{18h_y^2}+\frac{5}{18h_z^2} & \frac{25}{18h_x^2}+\frac{25}{18h_y^2}+\frac{25}{18h_z^2} \end{bmatrix} \tag{102}$$

$$\tilde{\boldsymbol{K}}^e_{23} = \begin{bmatrix} -\frac{1}{18h_x^2}-\frac{1}{18h_y^2}-\frac{1}{18h_z^2} & \frac{1}{18h_x^2}-\frac{5}{18h_y^2}-\frac{5}{18h_z^2} \\ \frac{1}{18h_x^2}-\frac{5}{18h_y^2}-\frac{5}{18h_z^2} & -\frac{1}{18h_x^2}-\frac{1}{18h_y^2}-\frac{1}{18h_z^2} \end{bmatrix} \tag{103}$$

$$\tilde{\boldsymbol{K}}^e_{24} = \begin{bmatrix} \frac{5}{18h_x^2}+\frac{5}{18h_y^2}-\frac{25}{18h_z^2} & -\frac{5}{18h_x^2}+\frac{1}{18h_y^2}-\frac{5}{18h_z^2} \\ -\frac{5}{18h_x^2}+\frac{1}{18h_y^2}-\frac{5}{18h_z^2} & \frac{5}{18h_x^2}+\frac{5}{18h_y^2}-\frac{25}{18h_z^2} \end{bmatrix} \tag{104}$$

$$\tilde{\boldsymbol{K}}^e_{33} = \begin{bmatrix} \frac{25}{18h_x^2}+\frac{25}{18h_y^2}+\frac{25}{18h_z^2} & -\frac{25}{18h_x^2}+\frac{5}{18h_y^2}+\frac{5}{18h_z^2} \\ -\frac{25}{18h_x^2}+\frac{5}{18h_y^2}+\frac{5}{18h_z^2} & \frac{25}{18h_x^2}+\frac{25}{18h_y^2}+\frac{25}{18h_z^2} \end{bmatrix} \tag{105}$$

$$\tilde{\boldsymbol{K}}^e_{34} = \begin{bmatrix} -\frac{5}{18h_x^2}-\frac{5}{18h_y^2}+\frac{1}{18h_z^2} & \frac{5}{18h_x^2}-\frac{25}{18h_y^2}+\frac{5}{18h_z^2} \\ \frac{5}{18h_x^2}-\frac{25}{18h_y^2}+\frac{5}{18h_z^2} & -\frac{5}{18h_x^2}-\frac{5}{18h_y^2}+\frac{1}{18h_z^2} \end{bmatrix} \tag{106}$$

$$\tilde{\boldsymbol{K}}^e_{44} = \begin{bmatrix} \frac{25}{18h_x^2}+\frac{25}{18h_y^2}+\frac{25}{18h_z^2} & -\frac{25}{18h_x^2}+\frac{5}{18h_y^2}+\frac{5}{18h_z^2} \\ -\frac{25}{18h_x^2}+\frac{5}{18h_y^2}+\frac{5}{18h_z^2} & \frac{25}{18h_x^2}+\frac{25}{18h_y^2}+\frac{25}{18h_z^2} \end{bmatrix} \tag{107}$$

The symbols D_i's in Eq. (76) are given by:

$$\begin{aligned} D_1 = & \left(-\frac{1}{2h_x^2}-\frac{1}{2h_y^2}-\frac{1}{2h_z^2}\right) d_{(A-1)(B-1)(C+1)} \\ & + \left(-\frac{5}{h_x^2}+\frac{1}{h_y^2}-\frac{5}{h_z^2}\right) d_{(A-1)(B-1)C} \\ & + \left(-\frac{1}{2h_x^2}-\frac{1}{2h_y^2}-\frac{1}{2h_z^2}\right) d_{(A-1)(B-1)(C-1)} \\ & + \left(\frac{1}{h_x^2}-\frac{5}{h_y^2}-\frac{5}{h_z^2}\right) d_{(A-1)B(C+1)} \\ & + \left(\frac{10}{h_x^2}+\frac{10}{h_y^2}-\frac{50}{h_z^2}\right) d_{(A-1)BC} \\ & + \left(\frac{1}{h_x^2}-\frac{5}{h_y^2}-\frac{5}{h_z^2}\right) d_{(A-1)B(C-1)} \end{aligned} \tag{108}$$

$$\begin{aligned} D_2 = & \left(-\frac{1}{2h_x^2}-\frac{1}{2h_y^2}-\frac{1}{2h_z^2}\right) d_{(A-1)(B+1)(C+1)} \\ & + \left(-\frac{5}{h_x^2}+\frac{1}{h_y^2}-\frac{5}{h_z^2}\right) d_{(A-1)(B+1)C} \\ & + \left(-\frac{1}{2h_x^2}-\frac{1}{2h_y^2}-\frac{1}{2h_z^2}\right) d_{(A-1)(B+1)(C-1)} \end{aligned}$$

$$
\begin{aligned}
&+\left(-\frac{5}{h_x^2}-\frac{5}{h_y^2}+\frac{1}{h_z^2}\right)d_{A(B-1)(C+1)}\\
&+\left(-\frac{50}{h_x^2}+\frac{10}{h_y^2}+\frac{10}{h_z^2}\right)d_{A(B-1)C}\\
&+\left(-\frac{5}{h_x^2}-\frac{5}{h_y^2}+\frac{1}{h_z^2}\right)d_{A(B-1)(C-1)}\\
&+\left(\frac{10}{h_x^2}-\frac{50}{h_y^2}+\frac{10}{h_z^2}\right)d_{AB(C+1)} \qquad (109)\\
D_3=&\left(\frac{100}{h_x^2}+\frac{100}{h_y^2}+\frac{100}{h_z^2}\right)d_{ABC}\\
&+\left(\frac{10}{h_x^2}-\frac{50}{h_y^2}+\frac{10}{h_z^2}\right)d_{AB(C-1)}\\
&+\left(-\frac{5}{h_x^2}-\frac{5}{h_y^2}+\frac{1}{h_z^2}\right)d_{A(B+1)(C+1)}\\
&+\left(-\frac{50}{h_x^2}+\frac{10}{h_y^2}+\frac{10}{h_z^2}\right)d_{A(B+1)C}\\
&+\left(-\frac{5}{h_x^2}-\frac{5}{h_y^2}+\frac{1}{h_z^2}\right)d_{A(B+1)(C-1)}\\
&+\left(-\frac{1}{2h_x^2}-\frac{1}{2h_y^2}-\frac{1}{2h_z^2}\right)d_{(A+1)(B-1)(C+1)} \qquad (110)\\
D_4=&\left(-\frac{5}{h_x^2}+\frac{1}{h_y^2}-\frac{5}{h_z^2}\right)d_{(A+1)(B-1)C}\\
&+\left(-\frac{1}{2h_x^2}-\frac{1}{2h_y^2}-\frac{1}{2h_z^2}\right)d_{(A+1)(B-1)(C-1)}\\
&+\left(\frac{1}{h_x^2}-\frac{5}{h_y^2}-\frac{5}{h_z^2}\right)d_{(A+1)B(C+1)}\\
&+\left(\frac{10}{h_x^2}+\frac{10}{h_y^2}-\frac{50}{h_z^2}\right)d_{(A+1)BC}\\
&+\left(\frac{1}{h_x^2}-\frac{5}{h_y^2}-\frac{5}{h_z^2}\right)d_{(A+1)B(C-1)}\\
&+\left(-\frac{1}{2h_x^2}-\frac{1}{2h_y^2}-\frac{1}{2h_z^2}\right)d_{(A+1)(B+1)(C+1)}\\
&+\left(-\frac{5}{h_x^2}+\frac{1}{h_y^2}-\frac{5}{h_z^2}\right)d_{(A+1)(B+1)C}\\
&+\left(-\frac{1}{2h_x^2}-\frac{1}{2h_y^2}-\frac{1}{2h_z^2}\right)d_{(A+1)(B+1)(C-1)} \qquad (111)
\end{aligned}
$$

The symbols $\mathcal{S}$ and $\mathcal{T}$ in Eq. (78) read:

$$
\begin{aligned}
\mathcal{S}=&\cos(-k_xh_x+k_yh_y-k_zh_z)\\
&+10\cos(-k_xh_x-k_zh_z)+\cos(-k_xh_x-k_yh_y-k_zh_z)\\
&+100\cos(-k_zh_z)+10\cos(k_yh_y-k_zh_z)\\
&+10\cos(-k_yh_y-k_zh_z)+10\cos(k_xh_x-k_zh_z)\\
&+\cos(k_xh_x+k_yh_y-k_zh_z)\\
&+\cos(k_xh_x-k_yh_y-k_zh_z)+10\cos(-k_xh_x+k_yh_y)\\
&+100\cos(-k_xh_x)+10\cos(-k_xh_x-k_yh_y)\\
&+100\cos(k_yh_y)+500 \qquad (112)\\
\mathcal{T}=&-\left(\frac{1}{h_x^2}+\frac{1}{h_y^2}+\frac{1}{h_z^2}\right)\cos\left(k_xh_x-k_yh_y+k_zh_z\right)\\
&-\left(\frac{10}{h_x^2}-\frac{2}{h_y^2}+\frac{10}{h_z^2}\right)\cos\left(k_xh_x+k_zh_z\right)\\
&-(\frac{1}{h_x^2}+\frac{1}{h_y^2}+\frac{1}{h_z^2})\cos(k_xh_x+k_yh_y+k_zh_z)\\
&+\left(\frac{2}{h_x^2}-\frac{10}{h_y^2}-\frac{10}{h_z^2}\right)\cos(k_yh_y-k_zh_z)\\
&+\left(\frac{20}{h_x^2}+\frac{20}{h_y^2}-\frac{100}{h_z^2}\right)\cos(k_zh_z)\\
&+\left(\frac{2}{h_x^2}-\frac{10}{h_y^2}-\frac{10}{h_z^2}\right)\cos(k_yh_y+k_zh_z)\\
&-\left(\frac{1}{h_x^2}+\frac{1}{h_y^2}+\frac{1}{h_z^2}\right)\cos(k_xh_x+k_yh_y-k_zh_z)\\
&-\left(\frac{10}{h_x^2}-\frac{2}{h_y^2}+\frac{10}{h_z^2}\right)\cos(k_xh_x-k_zh_z)\\
&-\left(\frac{1}{h_x^2}+\frac{1}{h_y^2}+\frac{1}{h_z^2}\right)\cos\left(k_xh_x-k_yh_y-k_zh_z\right)\\
&+\left(-\frac{10}{h_x^2}-\frac{10}{h_y^2}+\frac{2}{h_z^2}\right)\cos(k_xh_x-k_yh_y)\\
&+\left(-\frac{100}{h_x^2}+\frac{20}{h_y^2}+\frac{20}{h_z^2}\right)\cos(k_xh_x)\\
&+\left(-\frac{10}{h_x^2}-\frac{10}{h_y^2}+\frac{2}{h_z^2}\right)\cos(k_xh_x+k_yh_y)\\
&+\left(\frac{20}{h_x^2}-\frac{100}{h_y^2}+\frac{20}{h_z^2}\right)\cos(k_yh_y)\\
&+\frac{100}{h_x^2}+\frac{100}{h_y^2}+\frac{100}{h_z^2} \qquad (113)
\end{aligned}
$$

References

1. Hughes TJR (2000) The finite element method: linear static and synamic finite element analysis. Dover Publications, Mineola
2. Zienkiewicz OC, Taylor RL, Zhu JZ (2005) The finite element method: its basis and fundamentals. Elsevier, Singapore
3. Archer JS (1965) Consistent mass matrix formulation for structural analysis using finite element techniques. AIAA J 3:1910–1918
4. Fried I, Malkus DS (1975) Finite element mass matrix lumping by numerical integration with no convergence rate loss. Int J Solids Struct 11:461–466
5. Hintion E, Rock T, Zienkiewicz OC (1976) A note on mass lumping and related processes in the finite element method. Earthq Eng Struct Dyn 4:245–249
6. Cohen G, Joly P, Tordjman N (1994) Higher-order finite elements with mass-lumping for the 1D wave equation. Finite Elem Anal Des 16:329–336
7. Hu YC, Sze KY, Zhou YX (2015) Stabilized plane and axisymmetric Lobatto finite element models. Comput Mech 56:879–903
8. Bos L, Taylor MA, Wingate BA (2000) Tensor product Gauss-Lobatto points are Fekete points for the cube. Math Comput 70:1543–1547
9. Maday Y, Patera AT (1989) Spectral element methods for the incompressible Navier–Stokes equations. In: Noor AK (ed) State of the art surveys in computational mechanics. ASME, New York, pp 71–143
10. Komatitsch D, Vilotte JP (1998) The spectral element method: an efficient tool to simulate the seismic response of 2D and 3D geological structures. Bull Seismol Soc Am 88:368–392
11. Wu ZJ, Li FM (2016) Spectral element method and its application in analyzing the vibration band gap properties of two-dimensional square lattices. J Vib Control 22:710–721
12. Strang G, Fix GJ (1973) An analysis of the finite element method. Prentice-Hall, Englewood Cliffs
13. Stavrinidis C, Clinckemaillie J, Dubois J (1989) New concepts for finite element mass matrix formulations. AIAA J 27:1249–1255
14. Kim K (1993) A review of mass matrices for eigenproblems. Comput. Struct. 46:1041–1048
15. Felippa CA, Guo Q, Park KC (2015) Mass matrix templates: general description and 1D examples. Arch Comput Methods Eng 22:1–65
16. Goudreau GL (1970) Evaluation of discrete methods for the linear dynamic response of elastic and viscoelastic solids. UC SESM Report 69-15, University of California, Berkeley
17. Goudreau GL, Taylor RL (1973) Evaluation of numerical integration methods in elastodynamics. Comput Methods Appl Mech Eng 2:69–97
18. Belytschko T, Mullen R (1978) On dispersive properties of finite element solutions. In: Miklowitz J, Achenbach JD (eds) Modern problems in elastic wave propagation. Wiley, New York, pp 67–82
19. Fried I (1979) Accuracy of string element mass matrix. Comput Methods Appl Mech Eng 20:317–321
20. Christon MA (1999) The influence of the mass matrix on the dispersive nature of the semi-discrete, second-order wave equation. Comput Methods Appl Mech Eng 173:147–166
21. Fried I, Chavez M (2004) Superaccurate finite element eigenvalue computation. J Sound Vib 275:415–422
22. Dokumaci E (2006) On superaccurate finite elements and their duals for eigenvalue computation. J Sound Vib 298:432–438
23. Gurtin M (1972) The linear theory of elasticity. In: Truesdell C (ed) Encyclopedia of physics, vol II. Springer, Berlin, pp 1–295
24. Hansson PA, Sandberg G (1997) Mass matrices by minimization of modal errors. Int J Numer Methods Eng 40:4259–4271
25. Ahmadian H, Friswell MI, Mottershead JE (1998) Minimization of the discretization error in mass and stiffness formulations by an inverse method. Int J Numer Methods Eng 41:371–387
26. Ahmadian H, Farughi S (2011) Development of super-convergent plane stress element formulation using an inverse approach. Finite Elem Anal Des 47:796–803
27. Olovsson L, Simonsson K, Unosson M (2005) Selective mass scaling for explicit finite element analysis. Int J Numer Methods Eng 63:1436–1445
28. Tkachuk A, Bischoff M (2013) Variational methods for selective mass scaling. Comput Mech 52:563–570
29. Cocchetti G, Pagani M, Perego U (2015) Selective mass scaling for distorted solid-shell elements in explicit dynamics: optimal scaling factor and stable time step estimate. Int J Numer Methods Eng 101:700–731
30. Felippa CA (2000) Recent advances in finite element templates. In: Topping BHV (ed) Computational mechanics for the twenty-first century. Saxe-Coburn Publications, Edinburgh, pp 71–98
31. Felippa CA (2001) Customizing the mass and geometric stiffness of plane thin beam elements by Fourier methods. Eng Comput 18:286–303
32. Felippa CA (2006) Construction of customized mass-stiffness pairs using templates. J Aerosp Eng 19:241–258
33. Fried I, Leong K (2005) Superaccurate finite element eigenvalue via a Rayleigh quotient correction. J Sound Vib 288:375–386
34. Hughes TJR, Cottrell JA, Bazilevs Y (2005) Isogeometric analysis: CAD, finite elements, NURBS, exact geometry and mesh refinement. Comput Methods Appl Mech Eng 194:4135–4195
35. Cottrell JA, Reali A, Bazilevs Y, Hughes TJR (2006) Isogeometric analysis of structural vibrations. Comput Methods Appl Mech Eng 195:5257–5296
36. Hughes TJR, Evans JA, Reali A (2014) Finite element and NURBS approximations of eigenvalue, boundary-value, and initial-value problems. Comput Methods Appl Mech Eng 272:290–320
37. Wang D, Liu W, Zhang H (2013) Novel higher order mass matrices for isogeometric structural vibration analysis. Comput Methods Appl Mech Eng 260:92–108
38. Wang D, Liu W, Zhang H (2015) Superconvergent isogeometric free vibration analysis of Euler-Bernoulli beams and Kirchhoff plates with new higher order mass matrices. Comput Methods Appl Mech Eng 286:230–267
39. Wang D, Liang Q, Zhang H (2016) A superconvergent isogeometric formulation for eigenvalue computation of three dimensional wave equation. Comput Mech 57:1037–1060
40. Hughes TJR, Tezduyar TE (1984) Stability and accuracy analysis of some fully discrete algorithms for the one-dimensional second-order wave equation. Comput Struct 19:665–668
41. Guddati MN, Yue B (2004) Modified integration rules for reducing dispersion error in finite element methods. Comput Methods Appl Mech Eng 193:275–287
42. Rao SS (2007) Vibration of continuous systems. Wiley, Hoboken
43. Asmar NH (2005) Partial differential equations with Fourier series and boundary value problems, 2nd edn. Prentice Hall, New York